Perspectives of quantum annealing: methods and implementations

View the article online for updates and enhancements.

Perspectives of quantum annealing: methods and implementations

Philipp Hauke[1,2,3] , **Helmut G Katzgraber**[4] , **Wolfgang Lechner**[5,6,11] , **Hidetoshi Nishimori**[7,8] **and William D Oliver**[9,10]

1 INO-CNR BEC Center and Department of Physics, University of Trento, 38123Povo (TN), Italy
2 Kirchhoff-Institute for Physics, Heidelberg University, 69120 Heidelberg, Germany
3 Institute for Theoretical Physics, Heidelberg University, 69120 Heidelberg, Germany
4 Microsoft Quantum, Microsoft Corporation, Redmond, WA 98052, United States of America
5 Institute for Theoretical Physics, University of Innsbruck, 6020 Innsbruck, Austria
6 Institute for Quantum Optics and Quantum Information, Austrian Academy of Sciences, 6020 Innsbruck, Austria
7 Institute of Innovative Research, Tokyo Institute of Technology, Nagatsuta-cho, Midori-ku, Yokohama 226-8503, Japan
8 Graduate School of Information Sciences, Tohoku University, Sendai 980-8579, Japan
9 Research Laboratory of Electronics, Massachusetts Institute of Technology, Cambridge, Massachusetts 02139, United States of America
10 MIT Lincoln Laboratory, 244 Wood Street, Lexington, Massachusetts 02420, United States of America

E-mail: Wolfgang.Lechner@uibk.ac.at

CrossMark

Abstract

Quantum annealing is a computing paradigm that has the ambitious goal of efficiently solving large-scale combinatorial optimization problems of practical importance. However, many challenges have yet to be overcome before this goal can be reached. This perspectives article first gives a brief introduction to the concept of quantum annealing, and then highlights new pathways that may clear the way towards feasible and large scale quantum annealing. Moreover, since this field of research is to a strong degree driven by a synergy between experiment and theory, we discuss both in this work. An important focus in this article is on future perspectives, which complements other review articles, and which we hope will motivate further research.

(Some figures may appear in colour only in the online journal)

1. Introduction

The last two decades have seen tantalizing progress in the engineering of quantum devices, raising the hope to realize quantum technologies based on precise control over large ensembles of microscopic quantum degrees of freedom [1–13]. Notable examples are small-scale prototypes of circuit (gate)-based quantum computers, which use logical gate operations on quantum bits (qubits). These devices, if ideally built to a large scale, are theoretically proven to be able to run certain quantum algorithms exponentially faster than any classical computer running classical algorithms [14]. However, gate-based quantum computers are extremely hard to scale up in practice [15], with current quantum processing units consisting of less than one hundred qubits. Even worse, the aforementioned statement assumes that these are perfect qubits; including error correction results in a large overhead when encoding logical variables in physical ones. Given these challenges, researchers have thus searched for less demanding

Corresponding Editor: Professor Maciej Lewenstein
11 The author to whom any correspondence should be addressed.

alternatives, which may enable solving certain problems of practical importance, hopefully efficiently given particular criteria. Over the history of classical computing, analog special-purpose machines may be seen to have heralded programmable digital universal silicon-based computers. While current quantum annealing devices operate with stoquastic Hamiltonians and limited coherence times, the challenges ahead are to realize scalable and coherent implementations with extended control over the qubits and at the same time develop novel protocols and methods to reach larger efficiency. In doing so, a main challenge will be to implement error correction schemes which have been pioneered in the last decade for adiabatic protocols [16–19]. The experimental challenges for this next generation quantum annealing devices will be thus similarly demanding as scaling up digital quantum computers. In this article, we present perspectives on adiabatic quantum optimization—and its extension that allows for incoherent and non-adiabatic processes, quantum annealing—in which remarkable experimental and theoretical advances are currently being observed[12].

Quantum annealing [22–24] has been designed to solve classical combinatorial optimization problems, with applications including computer science problems [25], classification [26], quantum chemistry [27, 28], machine learning [29–31], search engine ranking [32, 33], protein folding [34], compressive sensing [35], molecular similarity in chemistry [28], the optimal trading trajectory problem [36], circuit fault diagnosis [37, 38], planning [39], job-shop scheduling [40], variational autoencoders [41, 42], and data processing in high energy physics [43, 44].

Such optimization problems require the minimization of a cost function, a task that can be rephrased as finding the ground state of a classical Ising Hamiltonian H_0 [45] (for a review see [46]). Many problems of practical importance, however, have cost functions with a large number of local minima, corresponding to Ising Hamiltonians that are reminiscent of classical spin glasses [47–50]. These characteristics make it extremely difficult for classical algorithms to find the global minimum [24]. Quantum annealing was conceived as an alternative to solve this formidable task, based on the idea to elevate the classical Ising Hamiltonian H_0 to the quantum domain, i.e., by taking it to describe a collection of interacting qubits.

According to the adiabatic theorem of quantum mechanics [51, 52] (see also references [53–55]), the ground state of the classical Ising model can be found by initializing the system in the ground state of some initial Hamiltonian H_1, which is easy to prepare both theoretically and experimentally. H_1 is chosen such that it does not commute with H_0, and the system parameters are changed sufficiently slowly such that the Hamiltonian changes gradually from H_1 to H_0. More explicitly, the system is described by a time-dependent Hamiltonian (see figure 1).

$$H(t) = A(t)H_0 + B(t)H_1, \tag{1}$$
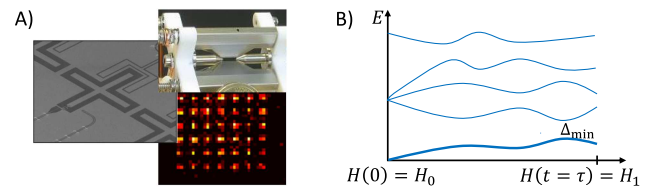
Figure 1. (A) Recent years have seen exciting developments on quantum-technology platforms (exemplified here by superconducting qubits, trapped ions, Rydberg atoms). These enable the implementation of quantum annealing protocols with the aim of solving hard optimization problems. (B) Sketch of time-dependent energy spectrum. The solution to the optimization problem is encoded in the ground state of a problem Hamiltonian H_0. It is reached at the end time τ of a slow sweep starting from the ground state of a Hamiltonian H_1 that is simple to prepare. If the sweep is sufficiently adiabatic (i.e., slow as compared to an inverse polynomial of the minimum gap $\Delta_{\min}$), the system remains in the instantaneous eigenstate throughout (thick line). This article discusses experimental as well as theoretical prospects to boost the performance of such quantum annealers. Picture credits panel A (clockwise from left): MIT Lincoln Laboratory; Blatt group, University of Innsbruck; LCF, Institut dOptique, CNRS.

where $B(t)$ is slowly reduced from the initial value $B(0) = 1$ to the final value $B(\tau) = 0$, with τ being the computation time, while $A(t)$ is slowly increased from $A(0) = 0$ to $A(\tau) = 1$, thus changing the Hamiltonian from $H(0) = H_1$ to $H(\tau) = H_0$. The adiabatic theorem states that, under a sufficiently slow change of the parameters in the Hamiltonian, the system ends up in a state close enough to the ground state of the final Hamiltonian H_0 if the initial condition is given as the ground state of the initial Hamiltonian H_1, meaning that the desired solution to the optimization problem is obtained. Since the final Hamiltonian H_0 is a classical Ising model with only commuting operators $\{\sigma_i^z\}$, the z component of the Pauli matrix, the solution can then be read out as the state of the individual qubits in the computational basis.

Thanks to the simplicity and elegance of this approach as well as its potential impact, several organizations including private companies are heavily investing efforts and resources toward its realization as large-scale quantum devices, mainly based on superconducting qubits [56–60]. Since the first quantum annealing devices by D-Wave Systems Inc. (called in the following "D-Wave devices") have become commercially available since 2011 [57], a large number of proof-of-principle demonstrations have appeared, though not in the adiabatic and coherent regime, see, e.g., references [61–69] and references therein.

Nevertheless, there is an ongoing scientific debate whether such quantum annealing devices can offer an actual speedup over classical computers [70–73]. In particular, a main consideration concerning a possible speedup is the closing of the minimal gap [74]. The adiabatic theorem determines a computational time that scales inversely proportional to a polynomial of the minimal energy gap. From this observation, the time scale of a fully adiabatic protocol is exponential for systems with a first order phase transition and polynomial for second order phase transitions. It was also shown that even in systems with a second order phase transition, exponentially

---

[12] We will also draw connections to another such example, namely special-purpose quantum computers known as quantum simulators, which may help researchers to solve quantum many-body problems [10, 11, 20, 21].

closing gaps can occur [75]. With this in mind, a desirable step in the field will be to lift the restriction of a naive adiabatic protocol.

For the case of the simple transverse-field Ising model, where we choose H_1 as the transverse field Hamiltonian $-\sum_{i=1}^{N} \sigma_i^x$, with σ_i^x being the Pauli matrix at qubit i, and where H_0 is written only in terms of $\{\sigma_i^z\}$, an essential speedup over classical algorithms may not be easy to achieve because equilibrium properties of the model, as well as certain aspects of dynamics, can usually be simulated efficiently by quantum Monte Carlo methods [76], although with some exceptions, e.g., reference [77]. This property of efficient simulatability is shared by a class of models called 'stoquastic Hamiltonians' [78], which are defined as those having a matrix representation with all off-diagonal elements being non-positive in a product basis, usually the computational basis to diagonalize $\{\sigma_i^z\}$, leading to a classical representation without the sign problem for simulations. The situation is further complicated by the presence of noise and a variety of imperfections in real devices, all of which degrade the performance, sometimes significantly. We also note that quantum annealing has triggered a variety of related protocols such as digitized quantum annealing [79], quantum approximate optimization [80], hybrid quantum–classical schemes [81, 82], thermally assisted annealing [83], to name a few.

In the present article, we aim to highlight new pathways and perspectives for the development of quantum annealing in the hope to clear the way towards establishment of feasible approaches for efficiently solving large-scale problems of practical importance. Therefore, an important focus of this article is on future perspectives, making its characteristics rather complementary to typical review articles [84–86]. Correspondingly, the list of references may be far from complete, for which we apologize to many authors.

This article is organized as follows. In section 2, we lay some theoretical framework of quantum annealing, starting from the representation of combinatorial optimization problems as classical Ising spin glasses, followed by an explanation of the essence of the adiabatic condition and the connection of the minimum energy gap to computational complexity. We also discuss how quantum annealing performs as compared to classical algorithms, and we point out the open question regarding the role of quantum entanglement in any possible quantum speedup. The core of the article consists of sections 3 and 4. In section 3, we highlight several promising routes towards enhancing the performance of quantum annealing based on improvements in algorithms. These include judicious choices of the quantum driving term H_1 and non-adiabatic schemes. In section 4, we discuss perspectives on the superconducting qubit platform and illustrate potential alternatives based on ultracold Rydberg atoms and trapped ions. Finally, we briefly summarize our discussions in section 5.

2. Theoretical framework

In this section, we recapitulate some of the theoretical framework that underlies the concept of quantum annealing, which will be useful for subsequent discussions.

2.1. From optimization problems to spin glasses

As stated in the Introduction, the main motivation for building quantum annealing machines such as the D-Wave device is to solve combinatorial optimization problems. Because in most cases only heuristic approaches to tackle these hard problems are known, there has been much interest in harnessing quantum effects in an attempt to find better solutions. Here, a 'better solution' can signify a cost closer to optimality, faster reaching of optimality at fixed cost, or a more diverse solution pool (if the problem has more than one minimizing configuration). Optimization problems can be cast in a form expressed in terms of binary (Boolean) variables $x_i \in \{0, 1\}$, generally as high-order polynomial unconstrained binary optimization problems (PUBO) written as k-local interactions with $k \geqslant 3$[13]. However, due to manufacturing constraints, current experimental devices can only handle 2-local interactions, i.e., *quadratic* unconstrained binary optimization problems (QUBOs) with a cost function of the form

$$H_{\text{QUBO}} = \sum_{ij} Q_{ij} x_i x_j + \sum_i c_i x_i. \tag{2}$$

The problem to be optimized is then fully specified by Q_{ij} and c_i. A broad class of paradigmatic optimization problems from vertex covers to the traveling salesperson problem have been mapped to QUBO form. For a comprehensive study, see reference [45].

If the problem of interest has a cost function of high-order interactions (k-local with $k \geqslant 3$), one should reduce it to QUBO format by using ancillary variables to implement it on a real device. For example, a 3-local expression $x_1 x_2 x_3$ is reduced to $x_1 x_4$ if we define $x_4 = x_2 x_3$. The latter condition can be imposed by an additional term in the cost function

$$3x_4 + x_2 x_3 - 2x_2 x_4 - 2x_3 x_4. \tag{3}$$

This expression is 0 only when $x_4 = x_2 x_3$ and is positive (higher cost) otherwise. Other expressions than equation (3) are possible for the same purpose with an appropriate coefficient for each term. While this technique has the advantage that any problem can in principle be studied on a currently-available device, it usually leads to a large overhead in the number of variables. Therefore, effort should further be made in studying combinatorial problems in their native PUBO form. We concentrate on QUBO in this article.

Equation (2) can be conveniently mapped to an Ising-like expression with the transformation $\sigma_i^z = 1 - 2x_i$:

$$H_{\text{SG}} = -\sum_{ij} J_{ij} \sigma_i^z \sigma_j^z - \sum_i h_i \sigma_i^z + \text{const.}, \tag{4}$$

where

$$J_{ij} = -\frac{1}{4} Q_{ij}, \tag{5}$$

$$h_i = -\frac{1}{2} \left(c_i + \sum_j Q_{ij} \right), \tag{6}$$

---

[13] A k-local interaction is a term in the cost function, the function to be minimized, proportional to a product of k binary variables, $x_{i_1} x_{i_2} \cdots x_{i_k}$.

and σ_i^z is regarded at this stage as a classical variable taking the values ± 1. The Hamiltonian H_{SG} is a typical example of the classical Ising Hamiltonian H_0 introduced in the Introduction. In equation (4) the constant (physically irrelevant) energy shift

$$E_0 = \frac{1}{4}\left(2\sum_i c_i + \sum_{ij} Q_{ij}\right) \qquad (7)$$

has been neglected. If the couplers J_{ij} are chosen from a random distribution, the Ising model given in equation (4) is also known as a spin glass. In what follows and without loss of generality, quantum annealing is discussed from the point of view of spin-glass Hamiltonians. We note, however, that the approach can be extended to other physical systems. There is a solid body of work on the disordered magnetic systems described as spin glasses, see, e.g., references [47–49, 87] and references therein. Yet, despite decades of study, our theoretical understanding is still insufficient, and simulations are restricted to small system sizes because the inherent frustration and disorder result in optimization problems of superb difficulty. This challenge has led to the development of sophisticated algorithms to study the thermodynamic behavior of classical spin glasses and, more recently, the adaptation of these methods as heuristics to minimize the energy of these systems [88–90]. We later discuss the performance of quantum annealing compared to these new, 'quantum inspired' optimization techniques.

In quantum annealing, the classical Ising variables σ_i^z are promoted to quantum spin operators, i.e., Pauli matrices. The solution to the optimization problem encoded in the ground state of equation (4) is then sought by slowly sweeping the system from a simple Hamiltonian H_1, whose ground state can be easily prepared and which does not commute with H_{SG}, to $H_0 = H_{SG}$, see equation (1). During this procedure, the probability to find a given classical configuration converges from a uniform distribution to a distribution that is ideally strongly peaked at the ground state of H_{SG}, see figure 2. In this context, the difficulty of solving the spin-glass problem translates into the presence of exponentially many energy gaps that are exponentially small once the annealing procedure enters the spin-glass phase [70, 75]. This makes quantum annealing a formidable task, for theoretical simulation and experimental realization alike. We note that the currently available annealing devices by D-Wave Systems Inc. are not operated in the strictly coherent adiabatic regime but are rather partly adiabatic, partly at finite-temperature equilibrium, and partly in the frozen regime [91].

Moreover, because the connectivity graph of the currently-available quantum annealers is limited, the study of any problem that does not happen to match, e.g., the underlying Chimera graph structure of the D-Wave device (see figure 3) requires 'embedding' [92], i.e., a representation of the logical optimization problem in the physically available graph structure. Typically, by use of strong Ising interactions, one locks a number of physical qubits together, such that they assume the same logical state. Neighbors of any of the physical qubits can thus interact with this new logical qubit. Effectively, one can thus engineer long-ranged interactions, irrespective of the
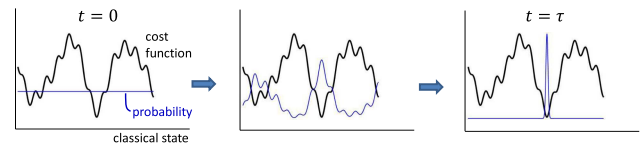

Figure 2. Sketch of quantum annealing protocol for a spin-glass problem. A typical spin-glass problem is characterized by a rough cost function (black line) as a function of the classical configurations, i.e., the energy eigenstates of the Ising Hamiltonian H_{SG} (ordered on *x*-axis). While the probability (blue line) to find any given classical state is uniform at the beginning of the annealing protocol, it converges to the desired solution at the end of the sweep, provided that the sweep is sufficiently adiabatic.
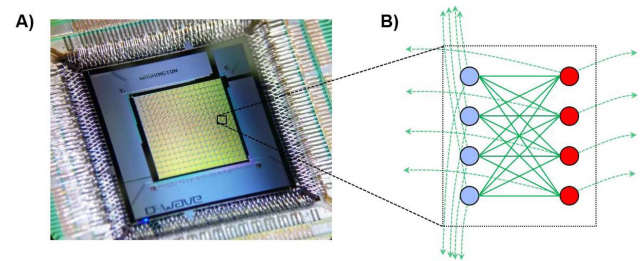

Figure 3. D-Wave 2000Q and the Chimera graph. (A) Photograph of a D-Wave 2000Q Washington chip with 2048 qubits. Media courtesy from D-Wave Systems Inc. [101]. (B) Chimera graph unit cell and connectivity. Bullets indicate qubits within the unit cell and solid lines connections between them. Dashed arrows indicate connections to adjacent unit cells, which are arranged in a square-lattice pattern.

underlying physical graph. This embedding, however, typically consumes a considerable overhead in terms of spin variables [93] and the method is limited as the strength required for the strong bonds increases with system size. For example, in the extreme case of a fully-connected graph, approximately 64 logical spin variables can be embedded in the 2000 variables of the D-Wave 2000Q quantum annealer. This overhead severely limits any asymptotic scaling analysis. As such, random spin-glass problems defined on the native Chimera lattice of the D-Wave device [56] have been extensively used to benchmark these machines, as well as quantum annealing in general [61–69].

An alternative encoding of optimization problems for quantum annealing is the LHZ (Lechner–Hauke–Zoller) scheme [94, 95]. In this architecture, the optimization problem is encoded in the local fields acting on the individual qubits, and all interactions are problem independent 4-body terms among nearest neighbors on a two dimensional grid. In this way, arbitrary optimization problems with programmable all-to-all interactions can be realized. The price to pay, however, also in this case is an overhead in the number of physical qubits compared to logical problem size. See section 3.2 for more details. Using LHZ, all-to-all models can be implemented in various platforms including transmon qubits [96], Kerr non-linear oscillators [97, 98], flux qubits [99] and Rydberg atoms [100] which will be discussed in section 4.3 in detail.

2.2. Adiabatic approximation and adiabatic theorem

As already suggested, the existence of quantum phase transitions and small energy gaps is one of the main sources of difficulties in quantum annealing. We describe this point in this and the following part of this section. In order to concisely elaborate the underlying principle, we assume here fully coherent dynamics.

One of the important theoretical bases of quantum annealing is the adiabatic approximation [51, 52]. The statement is that a quantum system with slowly time-dependent parameters in the Hamiltonian closely follows the instantaneous eigenstate in its time evolution if we start the dynamics in one of the eigenstates of the initial Hamiltonian [14]. Let us write the instantaneous eigenvalue equation of a Hamiltonian as

$$H(t)|j(t)\rangle = \epsilon_j(t)|j(t)\rangle, \tag{8}$$

where $j = 0$ denotes the instantaneous ground state and $j \geqslant 1$ represents instantaneous excited states. We assume for simplicity that states are discrete and non-degenerate. We note that the latter assumption may not be valid in general [102]. For a final Hamiltonian with a degenerate ground state, the adiabatic condition can never be satisfied and the final state can be studied from perturbation theory in the limit of small driver Hamiltonian using the Schrieffer–Wolff transformation [103–105].

In equation (8), the time variable t is fixed and is regarded as a parameter. The adiabatic approximation is concerned with the solution $|\psi(t)\rangle$ to the time-dependent Schrödinger equation generated by $H(t)$ with t now a dynamical variable. Our interest focuses mostly on the ground state, and thus we assume that the time evolution of the system starts from the ground state of the initial Hamiltonian $H(0) = H_1$, $|\psi(0)\rangle = |0(0)\rangle$. Then, the adiabatic approximation is that the wave function is considered to stay close to the instantaneous ground state after time evolution to $t = \tau$, $|\langle 0(\tau)|\psi(\tau)\rangle|^2 \approx 1$, as long as the adiabatic condition holds

$$\max_{0 \leqslant t \leqslant \tau} \frac{\left|\langle j(t)|\frac{\mathrm{d}H(t)}{\mathrm{d}t}|0(t)\rangle\right|}{\Delta_{j,0}(t)^2} \ll 1 \quad (j \geqslant 1). \tag{9}$$

Here, $\Delta_{j,0}(t) = \epsilon_j(t) - \epsilon_0(t)$ is the energy gap between the ground state and the jth excited state.

The adiabatic condition, equation (9), is derived from the evaluation of excitation probabilities and is not necessarily mathematically rigorous. Indeed, counterexamples are known in which the state of the system deviates significantly from the instantaneous ground state even when the adiabatic condition is satisfied. In particular, when the Hamiltonian has a time-dependent parameter with a time scale different from the intrinsic time scale related to the energy scale of the system, the system sometimes displays an oscillatory behavior even when the adiabatic condition, equation (9), is satisfied [52].

This last possibility is excluded if the time dependence of the Hamiltonian is parametrized by a single variable $s = t/\tau$,

where t changes from 0 to τ and accordingly s runs from 0 to 1, $\tilde{H}(s) \equiv H(t)$. If the Hamiltonian has this property, which is the case in most theoretical models of quantum annealing, the adiabatic condition equation (9) for $j = 1$ is rewritten as,

$$\tau \gg \max_{0 \leqslant s \leqslant 1} \frac{\left|\langle 1(s)|\frac{\mathrm{d}\tilde{H}(s)}{\mathrm{d}s}|0(s)\rangle\right|}{\Delta_{1,0}(s)^2}. \tag{10}$$

This equation gives an estimate of the computation time τ in terms of the minimum energy gap $\Delta_{\min} = \min_s \Delta_{1,0}(s)$ and is frequently used in theoretical analyses.

There exist several mathematically rigorous statements (adiabatic theorems) that give sufficient conditions for the system to stay sufficiently close to the instantaneous ground state [53–55, 106]. Nevertheless, since our interest is in the qualitative properties of the computation time τ as a function of the system size N, and rigorous adiabatic theorems lead to qualitatively the same conclusions, either polynomial or exponential time dependence of τ, we simply use the adiabatic condition of equation (10) in the following discussion.

2.3. Adiabatic quantum computing, adiabatic quantum optimization, and quantum annealing

Often, the framework of quantum computation that imposes the adiabatic condition equation (10), such that the system is supposed to always follow the instantaneous ground state, is called adiabatic quantum computing. The idea was first proposed in the context of a typical optimization problem of exact cover [107], and provides a framework that is known in its most general form to be theoretically equivalent to the traditional circuit (gate)-based model of quantum computing [108, 109]. Often, the term adiabatic quantum optimization is used to distinguish special optimization protocols from universal adiabatic quantum computing, where a quantum advantage is not necessarily proven.

Quantum annealing is a related concept [22][15]. It gives up the requirement of strict adiabatic processes and also allows for non-ideal situations including diabatic (non-adiabatic) transitions due to fast changes of Hamiltonian parameters as well as noisy environments of thermal and other origins. The computational power and possibility of a quantum advantage in this paradigm of quantum annealing is a matter of ongoing debate (see section 2.5). Nevertheless, the term quantum annealing is often used in the restricted sense of adiabatic processes, and we follow this tradition as long as it does not lead to a confusion.

2.4. Energy gap and computational complexity

As seen in equation (10), performance of quantum annealing strongly depends on the properties of the energy gap between ground and first excited states, $\Delta_{1,0}$, which should not be too small lest the necessary computation time τ becomes large or

---

[14] We distinguish the term 'adiabatic theorem' from 'adiabatic approximation', the former being reserved for rigorous mathematical theorems [53–55] whereas the latter is for approximations [51, 52].

[15] Several papers had proposed the term 'quantum annealing' [110–112] (see also [113, 114]) before reference [22] formulated quantum annealing in its current style. Those early papers used classical processes following, typically, the imaginary-time Schrödinger equation.

the system departs from the instantaneous ground state. However, the ground states of the initial and final Hamiltonians are qualitatively quite different because the initial state is supposed to be trivial, while the final state should encode a highly non-trivial optimization problem. This means that a phase transition occurs during the annealing procedure, and a quantum phase transition is known to be characterized by a vanishing energy gap in the thermodynamic limit [115].

Let us denote the minimum gap $\min_s \Delta_{1,0}(s)$ encountered during the annealing protocol as $\Delta_{\min}$. Suppose that this gap closes exponentially as a function of the system size, $\Delta_{\min} \propto e^{-cN}(c > 0)$, which occurs at a first-order quantum phase transition[16]. The order of magnitude of the numerator on the left-hand side of equation (10) is the same as that of the Hamiltonian, i.e., $\mathcal{O}(N)$, and thus can be ignored in comparison with the much-stronger exponential dependence of the denominator. The computational complexity (the size dependence of the computation time) is then exponential, $\tau \propto e^{2cN}$. In this case, the problem is considered hard to solve for the adiabatic quantum protocol. If, on the other hand, the minimum gap closes polynomially $\Delta_{\min} \propto N^{-l}(l > 0)$, as is usually observed in a second-order phase transition according to finite-size scaling [119], then the computation time is polynomial $\tau \propto N^{2l+1}$ and the problem is considered easy. Therefore the size dependence of the gap and the order of transition play important roles in the analysis of quantum annealing in the adiabatic framework. Notice here that a phase transition is a phenomenon that occurs only in the thermodynamic limit. Nevertheless, the order of transition in this limit gives us important information on the computational complexity for large but finite-size problems[17].

Consequently, one approach to improving the performance of quantum annealing is by mitigating the gap closing, e.g., by inhomogeneous driving of the transverse fields [120, 121], see section 3.1.2. A judicious choice of the annealing schedule can also allow to reduce the total evolution time, but is complicated by the fact that the precise location of the minimal gap is in general unknown [122]. Another interesting idea to improve the performance of quantum annealers is to employ their open-system character to advantage, since incoherent processes do not depend on the energy gap [123].

2.5. Quantum annealing vs classical simulation

A driving force for the development of quantum annealers is the hope to outperform classical devices. Before one can compare quantum annealing to classical approaches, however, one must define the metrics to be used. There are two main tracks to compare the performance of algorithms: resource estimation and performance for specific tasks.

Resource estimation [124] amounts to determining the necessary resources a particular method needs to achieve a target value. These resources can be, for example, time, energy, or memory. The target value can either be a particular energy

threshold or the true optimum of a benchmark instance. In the case of quantum annealing, it has been common to use spin-glass-like Hamiltonians as benchmark problems with the resources measured being the time it takes to solve an ensemble of problems as a function of the size of the input (here, the number of variables). Most recently, it has been argued [69] that energy should be included in such metrics. In addition, careful definitions of speedup are needed between quantum and classical paradigms. The first careful definition of quantum speedup was done in reference [125], later extended in reference [67] to add more granularity.

One can also use specific tasks to evaluate the performance of an algorithm. For example, one could analyze the quality of the solutions, as well as how correlated or uncorrelated a set of solutions are when the algorithms are run multiple times. Multiple studies [126, 127] have shown that quantum annealing is intrinsically biased and is therefore not a good sampler. As such, we focus here on resource requirements. However, it is worth emphasizing that advanced control techniques as outlined in this review, as well as non-stoquastic drivers, might alleviate the sampling problem for selected problems.

There have been multiple studies on the performance of quantum annealing and quantum annealing machines [58, 62–65, 71, 128–143]. However, to date, it remains controversial if quantum annealing can provide any '*quantum speedup*' or not. Such a statement strongly depends on the benchmark problem used and, to date, there is no industrial application where quantum annealing outperforms classical heuristics to the best of our knowledge. To extend the scaling regime of the different benchmark studies, researchers have shifted their focus to simple basic spin-glass problems, ideally on the native topology of quantum annealing machines. Unfortunately, it was demonstrated that random spin-glass benchmarks [63] on sparse graphs might not be complex enough to observe any advantage [62, 64]. Efforts have recently been focused on synthetic benchmark problems constructed using planting methods [65, 143], post-selection [64, 142, 144], and gadgets [69, 145]. Despite all these efforts, only reference [69] has demonstrated a *constant* speedup of quantum annealing over the best available heuristics for a synthetic benchmark. However, a constant speedup can easily be overcome by better implementations of the classical heuristics on better classical hardware [146, 147].

Reference [67] performed a comprehensive analysis of quantum annealing compared to multiple classical heuristics using synthetic benchmark problems. Quantum annealing was outperformed by parallel tempering Monte Carlo [148, 149] with isoenergetic cluster updates [150, 151], as well as the Hamze–de Freitas–Selby heuristic [152, 153], and the hybrid cluster method [140]. Nevertheless, within the class of *sequential algorithms*, quantum annealing on the D-Wave device as well as simulated quantum annealing outperformed simulated annealing [154] and population annealing Monte Carlo [155–158], therefore being the most efficient sequential optimization method to date. However, if the best-known quantum inspired optimization methods [67–69, 159–161] are included, a different picture emerges. We emphasize that this

---

[16] A few exceptions are known [116–118].

[17] There are known instances of relevant optimization problems where the minimum gap, e.g., is polynomial for small systems and becomes a stretched exponential only for sufficiently large problem instances [75].

statement concerns standard quantum annealing with a simple transverse field driver and a simple annealing schedule.

Thus, a definite quantum speedup remains to be found, and it is an important goal of this article to present possible pathways for quantum annealing using advanced control parameters and more complex drivers that may point to a possible future direction toward unlocking the long sought-after quantum speedup over classical hardware.

2.6. Role of entanglement in quantum annealing

For various quantum technologies, especially quantum cryptography [162], quantum-enhanced metrology [163], entanglement has often been regarded as a resource that enables tasks beyond the capabilities of classical devices.

In the case of quantum annealing experiments, the presence of entanglement has been witnessed [164, 165], but these experiments did not show any direct connection to the success probability or any other figure of merit of the quantum annealer. As several theoretical investigations studying different measures for entanglement indicate, the maximal entanglement achieved during the sweep has no implication on the success probability or a quantum speedup [166, 167]. However, reference [166] found analytically that the entanglement that survives at the end of the sweep does give an upper bound on the success probability. That is, if the system does not manage to get rid of the entanglement, the final state cannot assume a unique classical configuration, and the probability to reach the Ising ground state is diminished. A second indication for the role of entanglement in quantum annealing comes from the numerical study of reference [168], where it was shown that matrix product states with a larger cutoff for the allowed entanglement (as measured by the bond dimension) perform better in a simulation of the annealing procedure. Nevertheless, much further work is needed in order to understand the role of entanglement and quantumness towards any quantum speedup in a quantum annealing device. It will be especially interesting to investigate possible connections to other quantum effects that have been proposed to play a role in quantum annealing, especially quantum tunneling (see, e.g., [70, 129]).

3. Perspectives on methods

Due to the difficulty of benchmarking quantum annealers for spin-glass problems numerically and experimentally, the ultimate gain possible by these quantum devices over classical machines is an unresolved question of current research [72, 73]. There are, however, various pathways towards boosting their performance, on the conceptual as well as on the experimental side. These represent the bulk of the rest of this article. This section treats perspectives on methods while those on physical implementations are discussed in section 4.

3.1. Improvements by non-traditional terms and parameter control

This section explains recent approaches to the improvement of the performance of quantum annealing, which use methods

that lie out of the traditional formulation of quantum annealing based on the control of a simple transverse field applied uniformly over all qubits.

3.1.1. Non-stoquastic Hamiltonians. Most theoretical and experimental studies of quantum annealing refer to the transverse-field Ising model with the Hamiltonian

$$H = A(t)H_0 - B(t)\sum_i \sigma_i^x, \tag{11}$$

where H_0 is the classical Ising model of equation (4). The Hamiltonian in equation (11) with non-negative $B(t)$ has all its off-diagonal elements real and non-positive on the standard basis to diagonalize σ_i^z ($\forall i$) (the computational basis). A Hamiltonian satisfying this condition is called 'stoquastic', a compound of 'stochastic' and 'quantum' [169].[18]

A stoquastic Hamiltonian can generally be simulated efficiently on a classical computer by the standard method of Trotter decomposition (see [172, 173] for exceptions), which leads to non-negative effective local Boltzmann factors [174]. This means that there is no sign problem, which plagues classical simulations of many non-trivial quantum-mechanical systems [174–176]. Another interesting property of a stoquastic Hamiltonian is that all coefficients of the ground-state wave function can be chosen to be non-negative in the standard basis, due to the Perron–Frobenius theorem, which excludes quantum interference effects in the wave function. These facts suggest the possibility that a stoquastic Hamiltonian may be devoid of essential quantum effects necessary for quantum advantage over classical algorithms. Related is the absence of a formal proof that the computational power of quantum annealing based on stoquastic Hamiltonians exceeds that of classical algorithms for specific problems with a few exceptions including the glued-tree problem [177], in which one ingeniously takes advantage of intermediate diabatic transitions. See also [178], where the non-standard adaptive measurements in the final state are shown to be useful to achieve quantum enhancement in stoquastic Hamiltonians. This latter development is worth further scrutiny to clarify the power of stoquastic Hamiltonians.

A non-stoquastic Hamiltonian has arbitrary signs (and even complex values) in off-diagonal elements in the standard basis. A typical example is the Hamiltonian

$$H = -\sum_{i,j} J_{ij}\sigma_i^z\sigma_j^z - \sum_i h_i\sigma_i^z - \sum_i \Gamma_i\sigma_i^x + \sum_{i,j} \gamma_{ij}\sigma_i^x\sigma_j^x, \tag{12}$$

where $\Gamma_i \geqslant 0$ and some of the coefficients γ_{ij} are positive [19]. Also, adiabatic quantum computing based on a non-stoquastic Hamiltonian of the form of equation (12) is known to be

---

[18] More precisely, a Hamiltonian is stoquastic if the off-diagonal elements can be chosen real and non-positive in a basis which is a product of local bases [170]. The existence/absence of such a basis is not necessarily trivial [170, 171].

[19] The local rotation $\sigma_i^x \to -\sigma_i^x$, $\sigma_i^y \to -\sigma_i^y$, $\sigma_i^z \to \sigma_i^z$ at some of the qubits i can change the sign of Γ_i and γ_{ij}. The Hamiltonian is non-stoquastic if some of $-\Gamma_i$ and γ_{ij} remain positive under any such transformations.

equivalent to gate-based quantum computation [109]. See also reference [108].

We are thus motivated to study both theoretically and experimentally the properties of non-stoquastic Hamiltonians. There exist, however, many obstacles because, for example, it is difficult to study numerically large-size spin-glass-like systems by classical simulations due to a large relaxation time even in the absence of the sign problem, see section 2.1. Experimentally, realizing strong, tunable transverse interactions is also challenging, particularly for artificial atoms that are engineered to emulate spin-1/2 systems. For example, in the case of superconducting qubits (see section 4.1) using inductive couplings, the engineered magnetic moments $I_{x,i}$ used to realize the $\gamma_{ij}\sigma_i^x\sigma_j^x$ term are themselves dependent on the external control fields applied during the annealing protocol. This can be contrasted with an ideal spin-1/2 system, for which the magnetic moment $\mu_{x,z}$ is independent of the externally-applied magnetic fields $B_{x,y,z}$. Even when the $I_{x,i}$ are appropriately compensated, the magnitude of the resulting engineered coupling may not be as large as desired without increased engineering complexity, for example, through additional coupling elements to enhance the maximal value of γ_{ij}.

Nevertheless, several theoretical results have been reported that reveal enhanced computational capabilities of non-stoquastic Hamiltonians. In references [179–182], it was shown that, in simple mean-field-type models, an additional *XX* term with positive coefficient as in equation (12) reduces first-order phase transitions present in the conventional transverse-field Ising model of equation (11) to a second order transition. As described in section 2.4, this change of the order of the phase transition means an exponential speedup relative to the stoquastic case.

More specifically, let us adopt the *p*-spin model as the cost function,

$$H_0 = -N\left(\frac{1}{N}\sum_{i=1}^N \sigma_i^z\right)^p, \tag{13}$$

where $p \geqslant 3$ is an integer. Although the ground state is trivial for this model—all spin up $\sigma_i^z = 1$ (and all spin down $\sigma_i^z = -1$ for *p* even)—the system undergoes a first-order phase transition if we use the conventional transverse field as the quantum driving Hamiltonian H_1. This means that quantum annealing cannot solve this simple problem [183]. It is nevertheless possible to avoid this difficulty by the introduction of an *XX* term with a positive coefficient [179],

$$H(s,\lambda) = -s\lambda N\left(\frac{1}{N}\sum_{i=1}^N \sigma_i^z\right)^p - (1-s)\sum_{i=1}^N \sigma_i^x$$
$$+ s(1-\lambda)N\left(\frac{1}{N}\sum_{i=1}^N \sigma_i^x\right)^2, \tag{14}$$

where *s* and λ are time-dependent parameters that change from $s = 0$, λ arbitrary at $t = 0$ to $s = \lambda = 1$ at $t = \tau$. The last term in equation (14) makes the Hamiltonian non-stoquastic in the
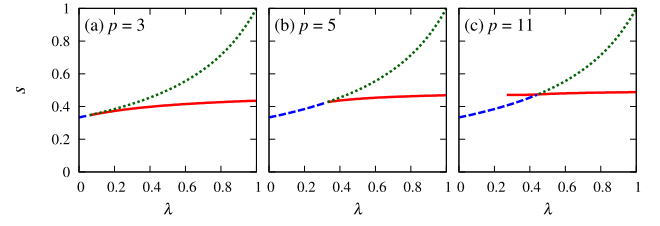

Figure 4. Phase diagram of the non-stoquastic *p*-spin model with (a) $p = 3$, (b) $p = 5$, and (c) $p = 11$. The red lines represent first-order transitions and the blue dashed lines are for second-order transitions. The green dotted lines above the red lines are extensions of the blue dashed lines and do not directly represent phase transitions. The small portion of second-order transitions for $p = 3$ near $\lambda = 0$ comes from finite-size effects [184]. Based on [179].

standard computational basis. Conventional quantum annealing is recovered for $\lambda = 1$, and $\lambda < 1$ represents the introduction of non-stoquastic effects. The phase diagram derived from statistical-mechanical calculations is displayed in figure 4. This figure shows that the line of first-order transitions (red solid line) terminates in the middle of the phase diagram and is replaced by a line of second-order transitions (blue dashed). It is thus possible to choose a path connecting the starting point $s = 0$, λ arbitrary and the final point $s = \lambda = 1$ without crossing a first-order transition. This means an exponential speedup relative to the conventional method that runs along the line $\lambda = 1$. Note that this speedup is not against best classical algorithms and also that an ingenious trick enables one to simulate classically this particular non-stoquastic Hamiltonian [185]. These notes notwithstanding, it is encouraging that an example exists that explicitly shows exponential performance enhancement by non-stoquastic Hamiltonians relative to the stoquastic counterpart. Also, a small-size spin glass problem was shown to have enhanced performance by a non-stoquastic Hamiltonian [186].

Though some efforts have begun to understand how non-stoquastic effects lead to enhanced performance [187], our knowledge is still primitive and more extensive studies should follow to reveal the computational power of non-stoquastic Hamiltonians, which may lead to essential quantum-mechanical enhancement even against classical algorithms.

3.1.2. Inhomogeneous driving of the transverse field. In conventional quantum annealing, the amplitude of a transverse field is controlled uniformly (homogeneously) over all qubits as in equation (11). As discussed in section 2.4, an adiabatic control of the homogeneous field from the initial value $B(0) = 1$ to $B(\tau) = 0$ causes a phase transition, which is one of the sources of difficulties. A control of the field that is inhomogeneous over space,

$$H = A(t)H_0 - B(t)\sum_i \Gamma_i \sigma_i^x, \tag{15}$$

where the amplitude Γ_i depends on *i*, may weaken the effects of a phase transition, because the number of qubits with the right critical values of coefficients for a phase transition to happen, $A(t)/(B(t)\Gamma_i) = $ critical, is reduced from macroscopic *N* for the uniform case ($\Gamma_i = 1\forall i$) to a much smaller number.

In other words, only a small portion of the system is at the phase transition point, and the effects of phase transition may be weakened. This is the basic idea of inhomogeneous driving of the transverse field.

References [188–191] studied the one-dimensional Ising model with an inhomogeneous field analytically based on the Kibble–Zurek mechanism [192, 193] and found evidence for better performance as measured by the number of defects (misaligned spins) in the final state. Numerical [194] and analytical [195, 196] work on typical combinatorial optimization problems of 3-SAT and maximum independent set problems also indicated improvements by inhomogeneity of the transverse field. Equilibrium statistical mechanical analysis of the *p*-spin model showed that the first-order phase transition is removed by the inhomogeneity of the transverse field [120, 121], which means an exponential speedup over the homogeneous protocol.

Following references [120, 121], let us choose in equation (15) the coefficients as $A(t) = t/\tau (\equiv s), B(t) = 1$, and the amplitude $\Gamma_i = 1$ for $i = 1, 2, \ldots, N(\tau - 1)(0 \leqslant \tau \leqslant 1)$ for qubits with field and $\Gamma_i = 0$ for $i = N(\tau - 1) + 1, \ldots, N$ for qubits without field, i.e.,

$$H = sH_0 - \sum_{i=1}^{N(1-\tau)} \sigma_i^x, \qquad (16)$$

where H_0 is the cost function of the *p*-spin model equation (13). Here, the parameter τ is for the ratio of qubits without transverse field (not to be confused with the computation time), and we start the annealing process with $s = \tau = 0 \left(H = -\sum_{i=1}^{N} \sigma_i^x \right)$ and end with $s(> 0)$ arbitrary and $\tau = 1$. The phase diagram is drawn in terms of these two parameters as in figure 5, where $\tau = 0$ represents the conventional protocol with transverse field homogeneously applied to all qubits. Each line represents a series of first-order transitions for a given *p*, starting from the $\tau = 0$ line and ending in the middle of the phase diagram. It is clearly possible to choose a path connecting the starting point $s = \tau = 0$ and ending at *s* arbitrary and $\tau = 1$, implying the existence of a way to switch off the field qubit by qubit as time *s* proceeds without hitting a phase transition. This means an exponential speedup as compared to the conventional method ($\tau = 0$) in the same sense as in the previous section for non-stoquastic Hamiltonians.

Experimentally, the current version of the D-Wave device features the option of an 'anneal offset,' which is to change the amplitude of the transverse field individually to some extent. Although it is not a complete realization of inhomogeneous field driving as described above, it nevertheless shows improved performance for some hard optimization problems [197]. In addition, it improves the biased sampling [127] that has been observed with standard transverse-field annealing protocols [164].

3.1.3. Reverse annealing. Reverse annealing is another protocol to control the amplitude of the transverse field in a
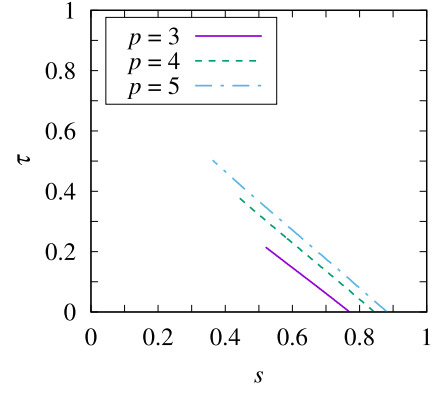

Figure 5. Phase diagram for the *p*-spin model under inhomogeneous field. Each line represents a series of first-order transitions for a given *p*, which extends to the middle of the phase diagram from the axis $\tau = 0$ corresponding to the conventional homogeneous field. Taken from [121].

non-traditional way. As proposed in reference [198] (see also [81]), we may be able to take advantage of partial knowledge on the correct solution, and use it as a candidate state expected to be close to the solution. Such a candidate may have been obtained by another method like classical simulations. We then start from this specific classical state under zero transverse field and increase the amplitude of the transverse field to a pre-assigned finite value and then decrease it again to zero. The system explores the space of states near the candidate state, which may be more efficient than the whole-space search from the *tabula rasa* initial condition in the traditional method.

Numerical results on a typical combinatorial optimization problem of 3-SAT indicate encouraging results [198]. An analysis of the *p*-spin model revealed that a first-order phase transition in the traditional formulation disappears by reverse annealing if the initial condition is chosen close to the correct solution [199]. In order to enforce the candidate state as the initial state, we add a term to the Hamiltonian of the *p*-spin model

$$H = sH_0 - (1-s)\lambda\sum_{i=1}^{N} \sigma_i^x - (1-s)(1-\lambda)\sum_{i=1}^{N} \epsilon_i\sigma_i^z, \quad (17)$$

where *s* and λ are parameters to control the time evolution, running from $s = \lambda = 0$ initially to $s = \lambda = 1$ finally. The parameter $\epsilon_i(= \pm 1)$ represents the candidate state, and the final term in the Hamiltonian equation (17) constrains the initial state to $\sigma_i^z = \epsilon_i (\forall i)$ at $s = \lambda = 0$. The ground state is trivial for the *p*-spin model ($\sigma_i^z = 1 (\forall i)$ for *p* odd and also $\sigma_i^z = -1 (\forall i)$ for *p* even), and ϵ_i is expected to be 1 with a probability *c* reasonably close to 1. In the phase diagram depicted in figure 6, the conventional quantum annealing (along the vertical line $\lambda = 1$) is seen to encounter a first order transition (blue curve) during the time evolution along the *s* axis. The line of first order transitions drawn blue terminates in the middle of the phase diagram if the initial condition is fairly close to the final solution, i.e. *c* close to 1 as in panels (b) and (c). This signifies an exponential speedup over the conventional approach along the line $\lambda = 1$.
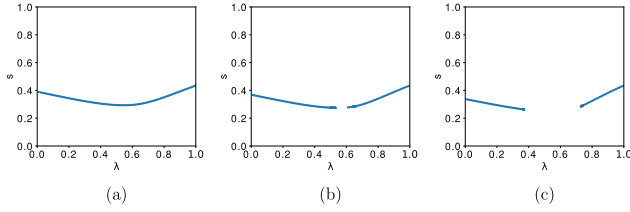
Figure 6. Phase diagrams on the λ–s plane for $p = 3$ and three values of c. The blue curves represent lines of first-order transitions. A path exists in (b) and (c) to connect the initial state at $s = \lambda = 0$ and the final state at $s = \lambda = 1$ without hitting a first order transition. Taken from [199]. (a) $c = 0.7$, (b) $c = 0.74$, (c) $c = 0.8$.

We note that reverse annealing is currently an active research field with the aim to improve the final ground state fidelity by tuning the schedule functions. Variations of reverse annealing include adiabatic reverse annealing [200], iterative reverse annealing [201] and paused annealing [91].

3.2. Non-adiabatic schemes

As discussed in section 2.2, the adiabatic condition poses a fundamental speed limit to adiabatic quantum optimization given by near-crossings of energy levels, making current implementations work in the regime where non-adiabatic transitions are important. A strategy to overcome this fundamental limitation is to leave the adiabatic approximation and introduce advantageously designed non-adiabatic methods, so-called counter-diabatic driving [202–206] and/or short-cut to adiabaticity [207–209]. Let us summarize the main idea of counter-diabatic driving.

We consider the frame rotating with respect to a unitary operator U and define the Hamiltonian in the rotating frame $\hat{\mathcal{H}} = U^\dagger \mathcal{H} U$ and the corresponding wave function $|\hat{\psi}\rangle = U^\dagger |\psi\rangle$. The Schrödinger equation is then

$$
\begin{aligned}
\hat{\mathcal{H}}|\hat{\psi}\rangle = i\hbar \partial_t |\hat{\psi}\rangle &= i\hbar \partial_t (U^\dagger |\psi\rangle) \\
&= i\hbar \partial_t \lambda \, \partial_\lambda U^\dagger |\psi\rangle + U^\dagger \mathcal{H} |\psi\rangle \\
&= \partial_t \lambda \, (i\hbar \partial_\lambda U^\dagger U)|\hat{\psi}\rangle + U^\dagger \mathcal{H} U |\hat{\psi}\rangle = (\hat{\mathcal{H}} - \dot{\lambda}\mathcal{A}_\lambda)|\hat{\psi}\rangle,
\end{aligned}
\tag{18}
$$

where we have defined the adiabatic gauge potential as

$$
\mathcal{A}_\lambda = i\hbar U^\dagger \partial_\lambda U. \tag{19}
$$

In the laboratory frame the gauge potential eliminates the off-diagonal terms of the moving Hamiltonian and thus any transition. This can be seen from differentiating $\hat{\mathcal{H}}(\lambda)$ with respect to λ. We obtain

$$
\partial_\lambda \hat{\mathcal{H}} = U^\dagger \partial_\lambda \mathcal{H} U + \frac{i}{\hbar}[\mathcal{A}_\lambda, \hat{\mathcal{H}}]. \tag{20}
$$

as $[\partial_\lambda \hat{\mathcal{H}}, \hat{\mathcal{H}}] = 0$. The adiabatic gauge potential $\mathcal{A}_\lambda$ from this equation is an exact formulation of the diabatic transition

due to a general unitary transformation. The idea of counter diabatic driving is to cancel this term by introducing the same term but with a negative sign in the Hamiltonian

$$
H_{\mathrm{CD}}(t) = H(t) + \dot{\lambda}\mathcal{A}_\lambda. \tag{21}
$$

Here, $H(t)$ is the original time-dependent Hamiltonian from the adiabatic quantum optimization protocol. In adding the exact counter-diabatic gauge potential, transitions get suppressed and the system remains in its instantaneous ground state for all times and sweeps [203].

However, from an experimental point of view, the exact gauge potential $\mathcal{A}_\lambda$ is of limited use, because the terms that appear in the Hamiltonian are highly non-local and include all orders of k-body interactions [203, 205]. It is thus a natural question whether one can find approximate counter-diabatic Hamiltonians that can be built with the available resources and still sufficiently improve the ground-state fidelity.

Recently, a variational method to find approximate counter-diabatic Hamiltonians has been introduced by Sels and Polknovnikov [205]. In this scheme, the recipe to construct approximate counter-diabatic terms is to use an ansatz that includes the experimental available interactions, which is then variationally optimized with respect to the adiabatic gauge potential. Here, we introduce $\mathcal{A}_\lambda^*$ as the approximate gauge potential which we variationally optimize. The idea is to minimize the operator distance between the exact gauge potential $\mathcal{A}_\lambda$ and the approximate ansatz gauge potential $\mathcal{A}_\lambda^*$ defined as

$$
D^2(\mathcal{A}_\lambda^*) = \mathrm{Tr}[(G_\lambda(\mathcal{A}_\lambda) - G_\lambda(\mathcal{A}_\lambda^*))^2] \tag{22}
$$

where the left-hand side is the Hilbert–Schmidt norm of the argument of the trace on the right-hand side with the definition

$$
G_\lambda(\mathcal{A}_\lambda^*) = \partial_\lambda H(t) + i[\mathcal{A}_\lambda^*, H(t)]. \tag{23}
$$

The aim is to minimize the operator distance with respect to the variational parameters of $\mathcal{A}_\lambda^*$ so that the approximate gauge potential is as close as possible to the exact gauge potential. In reference [205] it was shown that operator distance is equivalent to the minimum of the action

$$
\mathcal{S}(\mathcal{A}_\lambda^*) = \mathrm{Tr}[G_\lambda^2(\mathcal{A}_\lambda^*)] \tag{24}
$$

associated with the approximate adiabatic gauge potential $\mathcal{A}_\lambda^*$, i.e.,

$$
\frac{\delta \mathcal{S}(\mathcal{A}_\lambda^*)}{\delta \mathcal{A}_\lambda^*} = 0, \tag{25}
$$

where δ denotes the partial derivative.

In reference [205], this variational approach was demonstrated for a range of model systems, including an Ising spin chain. In this model, the counter-diabatic terms are derived from the ansatz

$$\mathcal{A}_\lambda^* = \sum_j \left[\alpha_j \sigma_j^y + \beta_j \left(\sigma_j^y \sigma_{j+1}^z + \sigma_j^z \sigma_{j+1}^y \right) \right. \tag{26}$$

$$\left. + \gamma_j \left(\sigma_j^y \sigma_{j+1}^x + \sigma_j^z \sigma_{j+1}^x \right) \right]. \tag{27}$$

Here, α, β and γ are functions of a switching function which interpolates the system parameter as

$$\lambda(t) = \lambda_0 + (\lambda_\mathrm{f} - \lambda_0)\sin^2\left(\frac{\pi}{2}\sin^2\left(\frac{\pi t}{2\tau} \right) \right), \tag{28}$$

where τ is the sweep time and λ_0 and λ_f are the initial and finals values, respectively. This particular form of the switching function is chosen to satisfy the condition that first and second derivatives at $t = 0$ and $t = \tau$ vanish. Adding a Hamiltonian term of the form of equation (27) with a switching function as in equation (28) to the standard annealing Hamiltonian improves the ground-state fidelity considerably. However, equation (27) consists of all-to-all $\sigma^y\sigma^x$ couplings if applied to a generic problem, which is experimentally challenging.

In reference [210], the variational counter diabatic terms have been combined with the LHZ implementation of all-to-all spin models [94]. The LHZ architecture encodes the optimization problem in local fields, as compared to the conventional Ising spin representation where the problem is encoded in pair interactions. The LHZ Hamiltonian reads as

$$H = A(t)\sum_i^K J_i \sigma_i^z + B(t)\sum_i^K \sigma_i^x + C(t)\sum_n^{K-N+1} C_n \sigma_i^z \sigma_j^z \sigma_k^z \sigma_l^z, \tag{29}$$

where A, B, and C are switching protocols, K is the number of connections (e.g., $K = N(N-1)/2$ for all-to-all models) and the indices in the last term run over four qubits in each plaquette of a square lattice.

The main result of reference [210] is a protocol to find optimal counter-diabatic terms with local qubit operations from a single-qubit ansatz for the counter-diabatic terms of the form $\mathcal{A}_\lambda^* = \sum_i \alpha_i \sigma_i^y$. The complete protocol is a quantum–classical hybrid approach where a variational parameter is updated from the outcome of a measurement from a quantum protocol. This protocol consists of two distinct variational optimizations: first, the analytical result from the gauge potential and second, the iterative optimization of a single optimization parameter from repeated measurements.

The possibility to loosen the strict adiabatic condition by using additional information about the system, be it variationally or analytically, may open the door to a wide range of theoretical and practical advances in adiabatic quantum optimization. Approximate counter-diabatic Hamiltonians may allow one to trade sweep time for available information about the problem and experimentally available resources.

4. Perspectives on implementations

Further theoretical advances are just one missing piece in order to arrive at quantum annealers that solve problems of practical relevance. Just as important will be a strong continued progress

in the design of quantum devices. In this section, we discuss the state of the art and future prospective of superconducting qubits, the paradigm platform for quantum annealing, as well as ideas for alternative platforms based on Rydberg atoms and trapped ions.

4.1. Superconducting qubits

Superconducting qubits are artificial spin-$1/2$ systems comprising lithographically defined inductors, capacitors, wires, and Josephson tunnel junctions. Their lithographic scalability, compatibility with electrical control signals, potential for high coherence, and the existence of a superconducting classical digital logic all converge to make the superconducting qubit modality the most advanced quantum annealers available today.

4.1.1. Current state-of-the-art and limitations. The current state-of-the-art for quantum annealers is the *D-Wave 2000Q* [101], a quantum annealing system comprising in excess of 2000 superconducting qubits and controlled in part by superconducting digital logic, see figure 3. The D-Wave 2000Q uses a 'Chimera graph' architecture [56], built around an 8-qubit unit cell. Each qubit has an *intra*-cell connectivity to four other qubits and *inter*-cell connectivity to two other qubits in neighboring unit cells. Problems are embedded on the Chimera architecture using proprietary software, and as mentioned in the Introduction, numerous examples have been implemented on D-Wave quantum annealers to date.

Despite D-Wave Systems Inc.'s truly remarkable engineering achievement, it remains unknown if the D-Wave quantum annealer—or quantum annealers in general—will afford quantum advantage for a general class of problems. The limitations of contemporary superconducting quantum annealers include:

- Short coherence times (compared with gate-model quantum computers).
- Limited connectivity (thus limiting the optimization problems that can be solved, see section 2.1, or requiring mappings such as the LHZ approach, equation (29)).
- Solely stoquastic (ZZ) coupling (thus excluding any potential advantage from non-stoquastic Hamiltonians, see section 3.1.1).
- Solely two-body interactions (hence precluding higher-order PUBOs, see section 2.1).
- Limited ability to tailor the annealing schedule for different qubits (hence limiting inhomogeneous-driving schemes, see section 3.1.2).

At the time of this writing, it is not known if remedying these limitations will practically lead to quantum advantage, but addressing them is a good place to start.

4.1.2. Introduction to superconducting qubits. As mentioned, superconducting qubits are lithographically defined circuits comprising inductors, capacitors, interconnects, and Josephson junctions [211]. When cooled to milliKelvin temperatures, these circuits exhibit quantized energy levels corresponding to quantized states of electric charge or magnetic
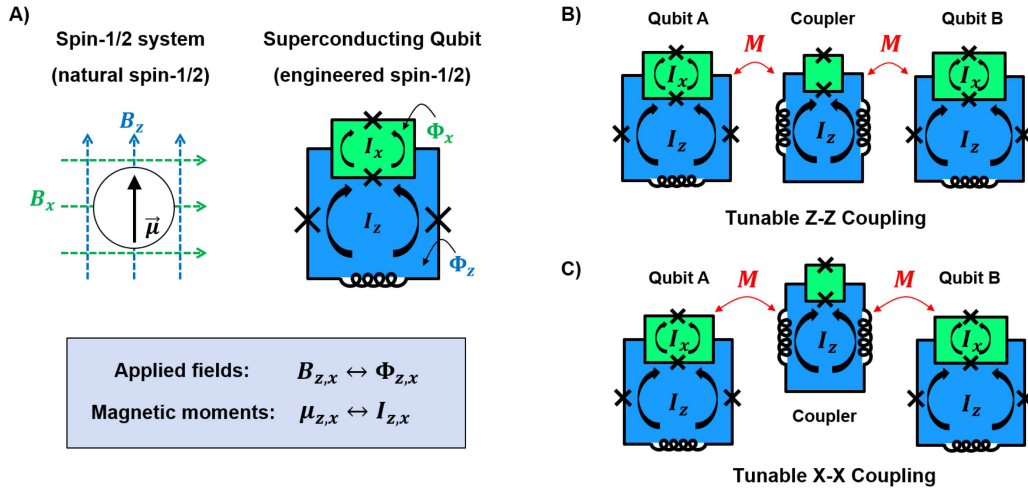
Figure 7. Superconducting qubits. (A) Comparison of an ideal spin-1/2 system and an engineered emulation of a spin-1/2 using a superconducting qubit. (B) Tunable Z–Z coupling mediated by an RF SQUID coupler. (C) Tunable X–X coupling mediated by an RF SQUID. This type of X–X coupling has limitations due to a field-dependent magnetic moment of the qubit.

flux, depending on the parameter values of these various circuit elements. In the context of gate-model quantum computation, the lowest-two of these energy levels are generally used as a quantum bit to represent logical states $|0\rangle$ and $|1\rangle$. Here, coherence within this reduced manifold is a premium, and, over the past 20 years, research groups worldwide have devoted significant resources to improving qubit coherence through a combination of materials, fabrication, and design advances. State of the art for gate-model qubits stands at approximately 100 μs for both the energy decay time (longitudinal relaxation time T_1) and coherence time (transverse relaxation time T_2) [212–215].

The approaches taken to achieve this level of coherence are often incompatible with the needs for quantum annealing. For example, qubits with fixed frequencies (determined during fabrication) or qubits with only σ^z tunability reduce the number of noise channels that can impact coherence, but do not allow for fully tunable transverse Ising Hamiltonians with σ^z and σ^x terms. Additionally, the materials (typically aluminum) and fabrication approaches (typically single-metal layers) are kept as simple and minimal as possible to avoid introducing unwanted defects that reduce T_1 and T_2, at the expense of circuit complexity. There are several types of gate-model qubits in common use today, including the transmon, capacitively shunted flux qubit, and fluxonium.

In contrast, the superconducting qubits used for quantum annealing are generally more complex by necessity. The most common type is called a 'X- and Z-tunable flux qubit,' comprising superconducting loops interrupted by Josephson junctions (indicated by the symbol 'X' in figure 7(A)) [216, 217]. In its conventional form, the Z-field is tunable by threading a magnetic field Φ_z through the σ^z-loop (blue). Clockwise and counterclockwise circulating currents are the two classical (diabatic) states of this circuit and serve to help screen Φ_z. When $\Phi_z = \Phi_0/2$, where $\Phi_0 = h/2e$ is the superconducting quantum unit of flux, both circulating-current states have the same energy and the system is frustrated. The green loop and its junctions serve to couple the diabatic currents,

opening an avoided crossing at this degeneracy point. The size of this avoided crossing, the strength of the X-field, is tunable by a magnetic flux Φ_x applied to the σ^x loop (green). In essence, the potential profile for this circuit is a two-dimensional double well. Each well corresponds to a circulating current, and the applied flux Φ_z tilts the wells. The wells are tunnel-coupled through a potential barrier, and the height of this barrier (and, thus, the tunneling rate) is tuned by the applied flux Φ_x.

Thus, an X- and Z-tunable flux qubit behaves as a spin-1/2 system in a magnetic field. The applied magnetic flux $\Phi_{x,z}$ and magnetic moment $I_{x,z} \times A_{x,z}$ of the flux qubit, where $A_{x,z}$ is the loop area, correspond to the applied field $B_{x,z}$ and magnetic moment $\mu_{x,z}$ of the natural spin-1/2, respectively. One important distinction, however, is that the magnetic moment I_x of the flux qubit is generally in Italic on the applied flux Φ_x. This should be contrasted with an ideal spin-1/2, for which the magnetic moment is constant and independent of the applied field. This difference must be compensated to realize ideal spin-1/2 behavior by either a careful calibration of the X-field and, more likely, additional complexity to realize the full range and strength of desired $\sigma_i^x \sigma_j^x$ coupling.

4.1.3. Approaches to coupling. Qubit coupling is achieved using mutual inductance between qubits and the qubit circulating currents. Although a direct interaction between qubits is possible in principle, it is not useful in practice, as the coupling strength cannot be tuned independently of the single-qubit field strengths. Rather, achieving large and tunable $\sigma_i^z \sigma_j^z$ and $\sigma_i^x \sigma_j^x$ coupling is implemented using intermediate qubits called 'couplers' (see figures 7(B) and (C)).

The couplers are qubits operated in a regime where they behave as tunable inductors with effective inductance L_{eff}. The X-field for the coupling is biased large enough that the coupler always remains in its ground state. Taking $\sigma_i^z \sigma_j^z$ coupling for example, the coupling energy J between two qubits, each with circulating current I_z and mutual coupling M, is $J = (I_z M)^2 / L_{\text{eff}}$. In turn, the inductance of the coupler is
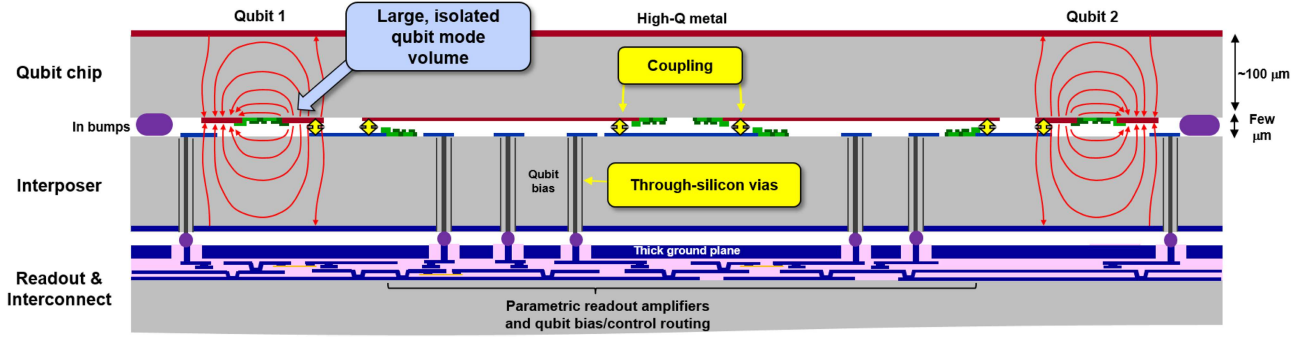
Figure 8. An approach to 3D integration that avoids the pitfalls of monolithic integration. Each chip in the stack—qubit chip, interposer, and readout & interconnect chip—is fabricated independently. The chips are then joined using indium bump-bonding. The approach enables high-coherence qubits in conjunction with addressability.

tunable using Φ_z^c applied to the coupler Z-loop, and the coupling can be tuned from ferromagnetic ($J < 0$) to antiferromagnetic ($J > 0$). For a detailed description of how this works, see references [59, 218]. A similar approach can be used to couple the X loops and achieve $\sigma_i^x \sigma_j^x$. By tuning the sign of the $\sigma_i^x \sigma_j^x$ coupling, one can realize both stoquastic and non-stoquastic Hamiltonians. Furthermore, the couplers themselves can be cascaded to achieve fanout [219]. We note that $\sigma_i^y \sigma_j^y$ coupling can also be realized using capacitive coupling.

There is a fundamental trade-off between strong coupling and high coherence. Large circulating currents lead to strong coupling, since $J \propto I_{x,z}^2$. However, coherence is severely impacted by the size of the circulating current and its corresponding magnetic moment. For example, the energy relaxation time scales as $1/I_{x,z}^2$ and the dephasing time scales as $1/I_{x,z}$ [59]. Thus, quantum annealers that use large circulating currents generally have low coherence times (around 10 ns), whereas gate-model qubits with high coherence (around 100 μs) all use small circulating currents [12]. The couplers can be used to compensate a weak coupling due to small circulating currents, and coupling strengths $J = 1$ GHz have been demonstrated using annealing qubits with coherence times around 1 μs [59].

4.1.4. 3D integration: coherence, connectivity, and tailored annealing. Current approaches to building quantum annealers generally use monolithic, multi-layer fabrication processes. The advantage of this approach is that it supports high levels of complexity, high connectivity, and the annealing protocol can be implemented on chip using superconducting control electronics, such as is done for the D-Wave 2000Q. However, this type of multi-layer fabrication exacerbates low coherence times due to the many fabrication steps required and the use of interwiring layer amorphous dielectrics. The result is an abundance of materials and fabrication-induced defects that sap coherence from the qubits.

An alternative approach was proposed in reference [60], and is called the 'three stack' (see figure 8). In this approach, there are three layers with unique functionalities, and each is fabricated separately. The qubit chip is fabricated in a high-coherence process similar to those used for gate-model qubits.

The readout and interconnect layer is a multi-layer process similar to conventional annealing processes; it can support dense interconnects, high connectivity, and active devices such as parametric amplifiers [220] and SFQ electronics [221]. To isolate this layer from the qubit chip, an interposer layer is introduced. The interposer is made of low-loss, intrinsic silicon and features superconducting through-silicon vias to bring signals from the readout and interconnect layer up to the qubit plane. By keeping the readout and interconnect layer far from the qubit chip, the electric and magnetic fields associated with the qubits are constrained to the low-loss qubit and interposer layers. The layers are then joined together using standard indium bump-bonding techniques.

With the three-stack or similar approaches, one can controllably study the impact of high coherence, high connectivity, and non-stoquastic coupling on the quantum annealing and its potential to achieve quantum advantage. Each layer can be fabricated independently and then combined in a manner that is itself extensible. This approach also supports both on-chip and off-chip control electronics, to enable annealing protocols that are tailored to each qubit and coupler individually. Once the key to achieving quantum advantage is understood, one can then focus on building larger machines using the most appropriate approach(es).

4.2. Trapped ions

While the mainstream platform for quantum annealing is superconducting qubits, with impressive progress in recent years, there do exist alternative systems. In particular, since atomic levels do not suffer from fabrication errors, quantum simulation platforms based on neutral or charged atoms represent promising alternatives in order to implement quantum annealers for practical applications or as highly-controlled test beds for fundamental questions. Examples include Rydberg atoms (see next section) and trapped ions, which we discuss in this section.

Charged ions [1] can be trapped by electromagnetic confining potentials in high vacuum, e.g., in linear Paul traps or Penning traps. The ions can then be cooled almost to the absolute ground state of their motional degrees of freedom, through which they arrange in regular crystal patterns due to their mutual Coulomb repulsion. The constituent qubits are
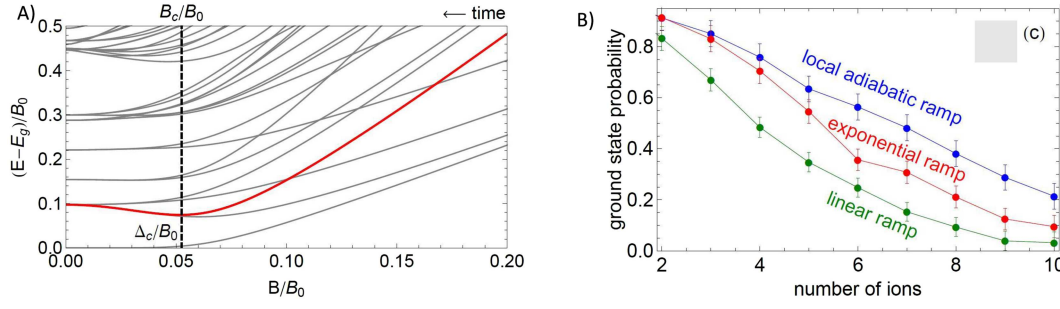
Figure 9. Adiabatic preparation of a spin-model ground in trapped ions, as reported in reference [230]. The model is described by the Hamiltonian $H = \sum_{i \neq j} J_{ij}\sigma_i^z\sigma_j^z + B(t)\sum_i \sigma_i^x$. (A) Energy levels E relative to the ground state E_g, computed for $N = 6$. The thick red line denotes the first excited level that gets coupled to the ground state and which defines the minimum gap Δ_c. The ramp begins at $B(t = 0) \equiv B_0 \gg \max(J_{ij})$, which also sets the energy scale. (B) For experimentally accessible ramp times, the overlap of the final state with the ground state rapidly decreases with system size. This effect can be mitigated by optimizing the ramp, for example, by being slower close to the minimum gap (denoted local adiabatic). Taken from reference [230].

encoded as two electronic hyperfine states, on which single-qubit rotations can be realized with extremely high fidelity by laser light or microwaves, depending on the chosen hyperfine states. These single-qubit terms can have arbitrary spatial dependence, thanks to single-ion addressing [222–224]. Due to the strength of the Coulomb repulsion, the distance between individual ions is typically on the order of a few micrometers, over which direct interactions between the hyperfine qubits are negligible. To introduce effective qubit–qubit interactions, one can couple the qubits off-resonantly via laser or microwave radiation to the collective phononic vibrations of the ion crystal [225–227]. Eliminating the phonons in second-order perturbation theory, the resulting interaction yields an Ising Hamiltonian with long-ranged coupling terms J_{ij} [222, 228–232].

Thus, including single-qubit rotations, the natural Hamiltonian for trapped-ion systems is

$$H = \sum_{i \neq j} J_{ij}(t)\sigma_i^z\sigma_j^z + \sum_i \sum_{\beta=x,y,z} B_i^\beta(t)\sigma_i^\beta. \qquad (30)$$

Time dependence of the Hamiltonian parameters is controlled simply by ramping laser intensities. This Hamiltonian thus provides all the ingredients for a basic annealing protocol.

As one limiting factor, the spatial dependence of the interactions J_{ij} is determined by the laser parameters, dimensionality of the crystal, and the phonon modes. If a single frequency μ is used to generate the interactions, they are typically given by [230]

$$J_{ij} \propto \Omega_i \Omega_j \sum_q \frac{\eta_i^q \eta_j^q}{\mu^2 - \omega_q^2}. \qquad (31)$$

Here, Ω_i is the laser Rabi frequency at ion i, ω_q is the frequency of the phonon mode q, and η_i^q is determined by the amplitude of the vibrational mode q at ion i.

In typical implementations, the frequency that generates the spin-spin interactions is tuned outside of the phonon band. For small systems,

$$J_{ij} \propto \frac{1}{|i - j|^\alpha} \qquad (32)$$

can then be approximated by a tunable powerlaw in the range $\alpha \in [0, 3]$ [232], while for larger systems it is better represented by a combination of an exponential and a dipolar decrease with distance [231]. Following a groundbreaking adiabatic protocol involving only two spins [233], quantum annealing with such long-range interactions and homogeneous fields has been realized with up to 18 qubits [229, 230] (although phrased in the context of quantum simulation and adiabatic state preparation of spin-model ground states). Though the trade-off between annealing speed and decoherence limited the overlap to the ground state at the end of the sweep, see figure 9, these experiments opened the road towards adiabatic protocols using trapped ions.

To proceed further on the road towards applications in quantum annealing, one requires besides engineering improvements (see below), the ability to freely program a desired optimization problem. In reference [166], it was shown that Hamiltonian equation (30) is sufficient to encode Coulomb glass problems as well as a variety of NP-complete models in a completely programmable manner, including the knapsack problem, number partitioning, and instances of the max-cut problem. To do this, one requires in addition to the programmable local rotations B_i^β only the ability to locally adjust the intensity Ω_i in equation (31). Both are experimentally feasible with existing single-site addressing-techniques using acousto-optic modulators or digital-mirror devices [223, 224]. An alternative approach to obtain benchmark models for quantum annealing is by generating deterministic instances of disordered spin-glass problems. This can be realized by tuning the radiation frequency μ into the phonon band [234], which generate interactions with high randomness and thus glassy behavior. Although the models resulting in this way may not be freely programmable, they can nevertheless provide valuable tests for quantum annealing protocols. Finally, if a number of frequencies that scales with the number of qubits is used to induce the qubit–qubit interactions, arbitrary interaction patterns J_{ij} can be programmed [235].

Regarding trap design and qubit coherence, there has been strong progress since the seminal experiments of reference [229, 230, 233]. Quantum simulations in linear Paul traps are now performed with tens of ions [236, 237]. Cryogenic traps will allow experimentalists to scale to 100 ions or more [238]. Numbers of this order are already being achieved in Penning traps [228], where adiabatic protocols in the Dicke model (an infinite-range spin model coupled to a bosonic mode) have recently been attempted for ~ 70 ions [239]. Segmented traps [240] and microfabricated surface traps [241–244] also open new possibilities for the design of interaction patterns. All the while, trapped-ion experiments are characterized by extremely large degrees of coherence. Life-times of the qubit levels are on the order of several seconds. Current limiting factors are fluctuations of magnetic fields and laser intensities. Often, these limit coherence times during the dynamics to several milliseconds, a time scale that is comparable to the one set by typical interaction strengths on the order of several kHz [236, 239]. By use of decoherence-free subspaces, these times can be increased to tens of milliseconds [222, 224].

As an interesting feature in this context, trapped ions allow for testing the effect of decoherence on the annealing protocol in a controlled manner. For example, by letting the local fields fluctuate in a temporally random way, dephasing noise can be simulated [166, 245]. Recently, it has been demonstrated that practically arbitrary noise spectral functions can be realized in this way, which has been used to study the effect of noise on quantum transport in a toy model for a photosynthetic complex [224]. It may be interesting to extend such analyses to true 'quantum baths', e.g., by resonant coupling to phonon modes as has been realized in a small toy model in reference [246]. Thus, the trapped-ion platform may provide a valuable test bed to benchmark quantum annealing subject to designed forms of decoherence.

4.3. Neutral atoms

Another ideal platform for quantum simulation in and out of equilibrium is Rydberg atoms, which offer large coherence times and individual control of qubits [247]. Using so-called dressing schemes [248], Rydberg atoms can implement Ising-spin models [249–252] with nearest neighbor interactions. In the context of adiabatic quantum optimization, a natural question is which models can be directly implemented in current neutral atom platforms, given that interactions are induced by laser-fields, which are challenging to tune individually.

In reference [100], the authors propose a Rydberg implementation for coherent quantum annealing based on the LHZ scheme [94], see equation (29). In this square lattice scheme, interactions are problem independent [C_n in equation (29)] and can thus be applied using a few lasers globally among all atoms. Local fields, which encode the optimization problem [J_i in equation (29)], can be applied with digital mirror devices with single site resolution. The main challenge in implementing LHZ is the realization of the required 4-body ZZZZ interactions. In reference [100], this issue is solved by a decomposition of the 4-body interactions into 2-body interactions with an overhead of one ancilla per plaquette. These ancilla atoms

are required to be of a different species (e.g., by combining Rb and Cs atoms), which poses an experimental challenge.

A direct implementation of the maximum independent set problem in neutral atoms was recently introduced in reference [253]. The maximum independent set of a graph is defined as the maximum set of vertices where no pair of vertices in each subset is connected by an edge. An experimental simplification can be achieved when restricting to unit disk graphs, which still leaves the problem NP-complete. These are planar graphs where vertices are placed on a two-dimensional grid and edges between vertices with a pair-wise distance smaller than a certain threshold. This problem can be directly mapped to Rydberg atoms using the so-called blockade mechanism, by which there exists a blockade radius around any atom that is excited to a Rydberg state within which no other atoms can be excited. Thus, the proposal serves as a direct test of quantum optimization without overhead from embedding.

As pointed out in section 2.1, a main challenge in quantum annealing is the infinite range interactions typical for hard optimization problems. In reference [254], the authors propose a direct implementation of an infinite range system with atoms in a cavity. The encoded problem is a variation of the N-Queens problem. The N-Queens problem is: given an $N \times N$ chess-board, place N queens such that no pieces attack each other (queens attack along rows, columns, and diagonals). A particular variation, the blocked-diagonals variation, is NP-complete and cannot be solved with current classical algorithms for $N > 21$. The problem can be mapped to an annealing protocol with N N-level systems. Each N-level system represents a column of the chess-board and each level a row. For example, if the second level of the third N-level system is occupied it means that a queen is placed on the second row of the third column on the chess board. The N-level systems are realized with atoms in one-dimensional optical lattices and the non-attacking condition is implemented with strong repulsive interactions along diagonals and rows. These interactions are mediated by the optical cavity and infinite range. The proposal is an attractive test bed for direct implementations of optimization problems. In particular, for this problem classical algorithms fail already for small numbers of atoms that will be available in near term. The proposal of reference [254] is based on coherence times limited to the order of 100 ms and interaction strengths of $Jt = 50$, which is the same order of magnitude as already demonstrated in experiment [255].

5. Summary

With the advent of intermediate scale quantum devices, we are currently witnessing the start of the second quantum revolution, where quantum mechanics will be used as a tool for computations tasks. With its relative simplicity and reduced demands on resources, quantum annealing may serve as a crucial stepping stone towards full-fledged quantum computing, not least by inciting reinvigorated experimental and theoretical efforts leading to a more precise engineering of quantum devices and a deeper understanding of quantum speedup. In this perspectives article, we have summarized possible routes

towards solving major open questions in the field of quantum annealing, including the question of possible quantum speedup from novel protocols, new encoding strategies that enable high coherent qubit platforms for quantum annealing, and novel hardware architectures that push the limits of coherence and control. Many promising routes to improved quantum annealing exist. Others that we have not discussed in this review include use of non-ergodic delocalized states [256], use of higher energy states where even stoquastic Hamiltonians can be universal [257], and hybrid quantum classical methods [258–261]. The field is still open and evolving rapidly, and we hope this article serves as a guideline for future research paving the way for quantum technology as a computational tool.

Acknowledgments

ORCID iDs

Philipp Hauke https://orcid.org/0000-0002-0414-1754
Helmut G Katzgraber https://orcid.org/0000-0003-3341-9943
Wolfgang Lechner https://orcid.org/0000-0003-3662-1020
William D Oliver https://orcid.org/0000-0001-8041-0824

References

[1] Kielpinski D, Monroe C and Wineland D J 2002 *Nature* **417** 709
[2] Blais A, Huang R S, Wallraff A, Girvin S M and Schoelkopf R J 2004 *Phys. Rev.* A **69** 062320
[3] Wallraff A, Schuster D I, Blais A, Frunzio L, Huang R S, Majer J, Kumar S, Girvin S M and Schoelkopf R J 2004 *Nature* **431** 162
[4] Schoelkopf R and Girvin S 2008 *Nature* **451** 664
[5] Clarke J and Wilhelm F K 2008 *Nature* **453** 1031
[6] Bakr W S, Gillen J I, Peng A, Fölling S and Greiner M 2009 *Nature* **462** 74
[7] Ladd T D, Jelezko F, Laflamme R, Nakamura Y, Monroe C and O'Brien J L 2010 *Nature* **464** 45
[8] O'Connell A D, Hofheinz M, Ansmann M, Bialczak R C, Lenander M, Lucero E, Neeley M, Sank D, Wang H and Weides M *et al* 2010 *Nature* **464** 697
[9] Chow J, DiCarlo L, Gambetta J, Nunnenkamp A, Bishop L S, Frunzio L, Devoret M, Girvin S and Schoelkopf R 2010 *Phys. Rev.* A **81** 062325
[10] Blatt R and Roos C F 2012 *Nat. Phys.* **8** 277
[11] Cirac J I and Zoller P 2012 *Nat. Phys.* **8** 264
[12] Yan F *et al* 2016 *Nat. Commun.* **7** 12303
[13] Bernien H *et al* 2017 *Nature* **551** 579
[14] Nielsen M A and Chuang I 2002 *Quantum Computation and Quantum Information* (Cambridge: Cambridge University Press)
[15] Preskill J 2018 *Quantum* **2** 79
[16] Young K C, Sarovar M and Blume-Kohout R 2013 *Phys. Rev. X* **3** 041013
[17] Pudenz K L, Albash T and Lidar D a 2014 *Nat. Commun.* **5** 3243
[18] Vinci W, Albash T and Lidar D A 2016 *npj Quantum Information* **2** 16017
[19] Marvian M and Lidar D A 2017 *Phys. Rev. Lett.* **118** 030504
[20] Hauke P, Cucchietti F M, Tagliacozzo L, Deutsch I and Lewenstein M 2012 *Rep. Prog. Phys.* **75** 082401
[21] Georgescu I M, Ashhab S and Nori F 2014 *Rev. Mod. Phys.* **86** 153
[22] Kadowaki T and Nishimori H 1998 *Phys. Rev. E* **58** 5355–63
[23] Farhi E, Goldstone J, Gutmann S and Sipser M 2000 Quantum computation by adiabatic evolution (arXiv:quant-ph/0001106)
[24] Kadowaki T 1998 Study of optimization problems by quantum annealing *PhD Thesis* Tokyo Institute of Technology arXiv:quant-ph/0205020
[25] Farhi E, Goldstone J, Gutmann S, Lapan J, Lundgren A and Preda D 2001 *Science* **292** 472–5
[26] Neven H, Denchev V S, Rose G and Macready W G 2009 arXiv:0912.0779
[27] Babbush R, Love P J and Aspuru-Guzik A 2014 *Sci. Rep.* **4** 6603
[28] Hernandez M and Aramon M 2017 *Quant. Inf. Proc.* **16** 133
[29] Lloyd S, Mohseni M and Rebentrost P 2013 arXiv:1307.0411
[30] Benedetti M, Realpe-Gómez J, Biswas R and Perdomo-Ortiz A 2016 *Phys. Rev. X* **7** 041052 (2017)
[31] Li R Y, Di Felice R, Rohs R and Lidar D A 2018 *NPJ Quantum Information* **4** 14
[32] Garnerone S, Zanardi P and Lidar D A 2012 *Phys. Rev. Lett.* **108** 230506
[33] Perdomo-Ortiz A, Dickson N, Drew-Brook M, Rose G and Aspuru-Guzik A 2012 *Sci. Rep.* **2** 571
[34] Perdomo-Ortiz A, Dickson N, Drew-Brook M, Rose G and Aspuru-Guzik A 2012 *Sci. Rep.* **2** 571
[35] Ayanzadeh R, Mousavi S, Halem M and Finin T 2019 arXiv:1901.00088
[36] Rosenberg G, Haghnegahdar P, Goddard P, Carr P, Wu K and de Prado M L 2016 *IEEE Journal of Selected Topics in Signal Processing* **10** 1053
[37] Perdomo-Ortiz A, Fluegemann J, Narasimhan S, Biswas R and Smelyanskiy V N 2015 *Eur. Phys. J. Spec. Top.* **224** 131

[38] Perdomo-Ortiz A *et al* 2017 *Phys. Rev. Applied* **12** 014004 (2019)

[39] Rieffel E G, Venturelli D, O'Gorman B, Do M B, Prystay E M and Smelyanskiy V N 2015 *Quant. Inf. Proc.* **14** 1

[40] Venturelli D, Marchand D J J and Rojo G 2015 arXiv:1506.08479

[41] Khoshaman A, Vinci W, Denis B, Andriyash E and Amin M H 2018 *Quantum Science and Technology* **4** 014001

[42] Wilson M, Vandal T, Hogg T and Rieffel E 2019 arXiv:1904.10573

[43] Mott A, Job J, Vlimant J R, Lidar D and Spiropulu M 2017 *Nature* **550** 375

[44] Das S, Wildridge A J, Vaidya S B and Jung A 2019 arXiv:1903.08879

[45] Lucas A 2014 *Front. Phys.* **12** 5

[46] Albash T and Lidar D A 2018 *Rev. Mod. Phys.* **90** 015002

[47] Binder K and Young A P 1986 *Rev. Mod. Phys.* **58** 801

[48] Young A P 1998 *Spin Glasses and Random Fields* (Singapore: World Scientific)

[49] Nishimori H 2001 *Statistical Physics of Spin Glasses and Information Processing: An Introduction* (Oxford: Oxford University Press)

[50] Mézard M, Parisi G and Virasoro M A 1987 *Spin Glass Theory and Beyond* (Singapore: World Scientific)

[51] Messiah A 1961 *Quantum Mechanics* (Amsterdam: North-Holland)

[52] Amin M H S 2009 *Phys. Rev. Lett.* **102** 220401

[53] Jansen S, Ruskai M B and Seiler R 2007 *J. Math. Phys.* **48** 102111

[54] Lidar D A, Rezakhani A T and Hamma A 2009 *J. Math. Phys.* **50** 102106

[55] Cheung D, Høyer P and Wiebe N 2011 *J. Phys. A: Math. Theor.* **44** 415302

[56] Bunyk P, Hoskinson E, Johnson M W, Tolkacheva E, Altomare F, Berkley A J, Harris R, Hilton J P, Lanting T and Whittaker J 2014 *IEEE Trans. Appl. Supercond.* **24** 1

[57] Johnson M W *et al* 2011 *Nature* **473** 194

[58] Dickson N G *et al* 2013 *Nat. Commun.* **4** 1903

[59] Weber S *et al* 2017 *Phys. Rev. Appl.* **8** 014004

[60] Rosenberg D *et al* 2017 *npj Quantum Information* **3** 42

[61] Albash T and Lidar D A 2018 *Phys. Rev. X* **8** 031016

[62] Katzgraber H G, Hamze F and Andrist R S 2014 *Phys. Rev. X* **4** 021008

[63] Rønnow T F, Wang Z, Job J, Boixo S, Isakov S V, Wecker D, Martinis J M, Lidar D A and Troyer M 2014 *Science* **345** 420 (2014)

[64] Katzgraber H G, Hamze F, Zhu Z, Ochoa A J and Munoz-Bauza H 2015 *Phys. Rev. X* **5** 031026

[65] Hen I, Job J, Albash T, Rønnow T F, Troyer M and Lidar D A 2015 *Phys. Rev. A* **92** 042325

[66] King A D, Lanting T and Harris R 2015 Performance of a quantum annealer on range-limited constraint satisfaction problems (arXiv:1502.02098)

[67] Mandrà S, Zhu Z, Wang W, Perdomo-Ortiz A and Katzgraber H G 2016 *Phys. Rev. A* **94** 022337

[68] Mandrà S and Katzgraber H G 2017 *Quantum Sci. Technol.* **2** 038501

[69] Mandrá S and Katzgraber H G 2018 *Quantum Sci. Technol.* **3** 04LT01

[70] Altshuler B, Krovi H and Roland J 2010 *Proc. Natl Acad. Sci.* **107** 12446

[71] Boixo S, Rønnow T F, Isakov S V, Wang Z, Wecker D, Lidar D A, Martinis J M and Troyer M 2014 *Nat. Phys.* **10** 218

[72] Rønnow T F, Wang Z, Job J, Boixo S, Isakov S V, Wecker D, Martinis J M, Lidar D A and Troyer M 2014 *Science* **345** 420–4

[73] Katzgraber H G 2018 Viewing vanilla quantum annealing through spin glasses *Quantum Sci. Technol.* **3** 030505 (2018)

[74] Jörg T, Krzakala F, Kurchan J and Maggs A 2008 *Phys. Rev. Lett.* **101** 147204

[75] Knysh S 2016 *Nat. Commun.* **7** 12370

[76] Isakov S V, Mazzola G, Smelyanskiy V N, Jiang Z, Boixo S, Neven H and Troyer M 2016 *Phys. Rev. Lett.* **117** 180402

[77] Andriyash E and Amin M H 2017 (arXiv:1703.09277)

[78] Bravyi S and Terhal B 2009 *SIAM J. Comput.* **39** 1462

[79] Barends R *et al* 2016 *Nature* **534** 222

[80] Farhi E, Goldstone J and Gutmann S 2014 arXiv:1411.4028

[81] Chancellor N 2017 *New J. Phys.* **19** 023024

[82] Battaglia D A, Santoro G E and Tosatti E 2005 *Phys. Rev.* E **71** 066707

[83] Dickson N G *et al* 2013 *Nat. Commun.* **4** 1903

[84] Albash T and Lidar D A 2018 *Rev. Mod. Phys.* **90** 015002

[85] Das A and Chakrabarti B K 2008 *Rev. Mod. Phys.* **80** 1061

[86] Venegas-Andraca S E, Cruz-Santos W, McGeoch C and Lanzagorta M 2018 *Contemp. Phys.* **59** 174–97

[87] Stein D L and Newman C M 2013 *Spin Glasses and Complexity Primers in Complex Systems* (Princeton NJ: Princeton University Press)

[88] Katzgraber H G and Young A P 2003 *Phys. Rev.* B **68** 224408

[89] Katzgraber H G, Körner M, Liers F, Jünger M and Hartmann A K 2005 *Phys. Rev.* B **72** 094421

[90] Zhu Z, Fang C and Katzgraber H G 2016 borealis—A generalized global update algorithm for Boolean optimization problems (arXiv:1605.09399)

[91] Marshall J, Venturelli D, Hen I and Rieffel E G 2019 *Phys. Rev. Appl.* **11** 044083

[92] Choi V 2008 *Quant. Inf. Proc.* **7** 193

[93] Zaribafiyan A, Marchand D J J and Changiz Rezaei S S 2017 *Quant. Inf. Proc.* **16** 1–26

[94] Lechner W, Hauke P and Zoller P 2015 *Sci. Adv.* **1** e1500838

[95] Rocchetto A, Benjamin S C and Li Y 2016 *Sci. Adv.* **2** e1601246

[96] Leib M, Zoller P and Lechner W 2016 *Quantum Science and Technology* **1** 015008

[97] Goto H 2015 *Sci. Rep.* **6** 21686

[98] Puri S, Andersen C K, Grimsmo A L and Blais A 2017 *Nat. Commun.* **8** 15785

[99] Chancellor N, Zohren S and Warburton P A 2017 *npj Quantum Information* **3** 21

[100] Glaetzle A W, van Bijnen R M, Zoller P and Lechner W 2017 *Nat. Commun.* **8** 15813

[101] D-Wave Systems https://dwavesys.com/

[102] Tayarani N M H and Prügel-Bennett A 2013 *IEEE Trans. Evol. Comput.* **18** 420–34

[103] Sieberer L M and Lechner W 2018 *Phys. Rev. A* **97** 052329

[104] Könz M S, Mazzola G, Ochoa A J, Katzgraber H G and Troyer M 2018 *Phys. Rev. A* **100** 030303 (2019)

[105] Dlaska C, Sieberer L M and Lechner W 2019 *Phys. Rev. A* **99** 032342

[106] Marzlin K P and Sanders B 2004 *Phys. Rev. Lett.* **93** 160408

[107] Farhi E, Goldstone J, Gutmann S, Lapan J, Lundgren A and Preda D 2001 *Science* **292** 472–6

[108] Aharonov D, van Dam W, Kempe J, Landau Z, Lloyd S and Regev O 2008 *SIAM Rev.* **50** 755–87

[109] Biamonte J and Love P 2008 *Phys. Rev. A* **78** 012352

[110] Apollini B, Cesa-Bianchi N and de Falco D 1988 *Proc. of the Ascona/Locarno Conf.* (Singapore: World Scientific)

[111] Apolloni B, Carvalho C and de Falco D 1989 *Stoch. Process. their Appl.* **33** 233–44

[112] Finnila A B, Gomez M A, Sebenik C, Stenson C and Doll J D 1994 *Chem. Phys. Lett.* **219** 343–8

[113] Amara P, Hsu D and Straub J 1993 *J. Phys. Chem.* **97** 6715–21

[114] Tanaka K and Horiguchi T 2000 *Electron. Commun. Jpn.* **83** 84–94

[115] Sachdev S 1999 *Quantum Phase Transitions* (Cambridge: Cambridge University Press)

[116] Cabrera G G and Jullien R 1987 *Phys. Rev.* B **35** 7061

[117] Laumann C R, Moessner R, Scardicchio A and Sondhi S L 2012 *Phys. Rev. Lett.* **109** 030502

[118] Tsuda J, Yamanaka Y and Nishimori H 2013 *J. Phys. Soc. Jpn.* **82** 114004

[119] Nishimori H and Ortiz G 2011 *Elements of Phase Transitions and Critical Phenomena* (Oxford: Oxford University Press)

[120] Susa Y, Yamashiro Y, Yamamoto M and Nishimori H 2018 *J. Phys. Soc. Jpn.* **87** 023002

[121] Susa Y, Yamashiro Y, Yamamoto M, Hen I, Lidar D A and Nishimori H 2018 *Phys. Rev.* A **98** 042326

[122] Zeng L, Zhang and Sarovar M 2015 *J. Phys. A: Math. Theor.* **49** 165305

[123] Amin M H 2015 *Phys. Rev.* A **92** 052323

[124] McGeoch C C 2012 *A Guide to Experimental Algorithmics* (Cambride: Cambridge University Press)

[125] Rønnow T F, Wang Z, Job J, Boixo S, Isakov S V, Wecker D, Martinis J M, Lidar D A and Troyer M 2014 *Science* **345** 420

[126] Matsuda Y, Nishimori H and Katzgraber H G 2009 *New J. Phys.* **11** 073021

[127] Mandrà S, Zhu Z and Katzgraber H G 2017 *Phys. Rev. Lett.* **118** 070502

[128] Santoro G, Martoňák R, Tosatti E and Car R 2002 *Science* **295** 2427

[129] Santoro G E and Tosatti E 2006 *J. Phys.* A **39** R393

[130] Pudenz K L, Albash T and Lidar D A 2014 *Nat. Commun.* **5** 3243

[131] Smith G and Smolin J 2013 *Physics* **6** 105

[132] Boixo S, Albash T, Spedalieri F M, Chancellor N and Lidar D A 2013 *Nat. Commun.* **4** 2067

[133] Lanting T *et al* 2014 *Phys. Rev.* X **4** 021041

[134] Santra S, Quiroz G, Ver Steeg G and Lidar D A 2014 *New J. Phys.* **16** 045006

[135] Shin S W, Smith G, Smolin J A and Vazirani U 2014 How 'Quantum' is the D-Wave machine? (arXiv:1401.7087)

[136] Albash T, Vinci W, Mishra A, Warburton P A and Lidar D A 2015 *Phys. Rev.* A **91** 042314

[137] Albash T, Rønnow T F, Troyer M and Lidar D A 2015 *Eur. Phys. J. Spec. Top.* **224** 111

[138] Martin-Mayor V and Hen I 2015 Unraveling quantum annealers using classical hardness *Scientific Reports* **5** 15324 (2015)

[139] Pudenz K L, Albash T and Lidar D A 2015 *Phys. Rev.* A **91** 042302

[140] Venturelli D, Mandrà S, Knysh S, O'Gorman B, Biswas R and Smelyanskiy V 2015 *Phys. Rev.* X **5** 031040

[141] Vinci W, Albash T, Paz-Silva G, Hen I and Lidar D A 2015 *Phys. Rev.* A **92** 042310

[142] Zhu Z, Ochoa A J, Hamze F, Schnabel S and Katzgraber H G 2016 *Phys. Rev.* A **93** 012317

[143] King J, Yarkoni S, Raymond J, Ozfidan I, King A D, Nevisi M M, Hilton J P and McGeoch C C 2017 arXiv:quant-phys/1701.04579

[144] Marshall J, Martin-Mayor V and Hen I 2016 *Phys. Rev.* A **94** 012320

[145] Denchev V S, Boixo S, Isakov S V, Ding N, Babbush R, Smelyanskiy V, Martinis J and Neven H 2016 *Phys. Rev.* X **6** 031015

[146] Matsubara S *et al* 2017 *Ising-Model Optimizer with Parallel-Trial Bit-Sieve Engine* (Cham: Springer International Publishing) p 432

[147] Aramon M, Rosenberg G, Miyazawa T, Tamura H and Katzgraber H G 2018 *Front. Phys.* **7** 48 (2019)

[148] Geyer C 1991 Monte Carlo maximum likelihood for dependent data *23rd Symp. on the Interface* ed E M Keramidas (Fairfax Station: Interface Foundation) p 156

[149] Hukushima K and Nemoto K 1996 *J. Phys. Soc. Jpn.* **65** 1604

[150] Houdayer J 2001 *Eur. Phys. J.* B **22** 479

[151] Zhu Z, Ochoa A J and Katzgraber H G 2015 *Phys. Rev. Lett.* **115** 077201

[152] Hamze F and de Freitas N 2004 *From Fields to Trees Proc. of the 20th Conf. on Uncertainty in Artificial Intelligence UAI '04* (Arlington: AUAI Press) p 243

[153] Selby A 2014 Efficient subgraph-based sampling of Ising-type models with frustration (arXiv:cond-mat/1409.3934)

[154] Kirkpatrick S, Gelatt C D Jr and Vecchi M P 1983 *Science* **220** 671

[155] Hukushima K and Iba Y 2003 *Population Annealing and its Application to a Spin Glass the Monte Carlo Method in the Physical Sciences: Celebrating the 50th Anniversary of the Metropolis Algorithm* Gubernatis J E (Los Alamos (USA): AIP) vol 690 p 200

[156] Machta J 2010 *Phys. Rev.* E **82** 026704

[157] Wang W, Machta J and Katzgraber H G 2015 *Phys. Rev.* E **92** 013303

[158] Wang W, Machta J and Katzgraber H G 2015 *Phys. Rev.* E **92** 063307

[159] Hartmann A K and Rieger H 2001 *Optimization Algorithms in Physics* (Berlin: Wiley-VCH)

[160] Elf M, Gutwenger C, Jünger M and Rinaldi G 2001 *Lecture Notes in Computer Science 2241 Computational Combinatorial Optimization* ed M Jünger and D Naddef (Heidelberg: Springer) vol 2241

[161] Hartmann A K and Rieger H 2004 *New Optimization Algorithms in Physics* (Berlin: Wiley-VCH)

[162] Gisin N, Ribordy G, Tittel W and Zbinden H 2002 *Rev. Mod. Phys.* **74** 145

[163] Pezzè L, Smerzi A, Oberthaler M K, Schmied R and Treutlein P 2018 *Rev. Mod. Phys.* **90** 035005

[164] Lanting T, King A D, Evert B and Hoskinson E 2017 *Phys. Rev.* A **96** 042322

[165] Albash T, Rønnow T F, Troyer M and Lidar D A 2015 *Eur. Phys. J. Spec. Top.* **224** 111–29

[166] Hauke P, Bonnes L, Heyl M and Lechner W 2015 *Front. Phys.* **3** 21

[167] Batle J, Ooi C R, Farouk A, Abutalib M and Abdalla S 2016 *Quant. Inf. Proc.* **15** 3081–99

[168] Bauer B, Wang L, Pižorn I and Troyer M 2015 arXiv:1501.06914

[169] Bravyi S, Divincenzo D P, Oliveira R and Terhal B M 2004 *Quantum Information and Computation* **8** 361–85

[170] Klassen J and Terhal B M 2018 *Quantum* **3** 139 (2019)

[171] Marvian M, Lidar D A and Hen I 2018 *Nature Comm.* **10** 1571 (2019)

[172] Hastings M B and Freedman M H 2013 *Quantum Information and Computation* **13** 1038–76

[173] Jarret M, Jordan S P and Lackey B 2016 *Phys. Rev.* A **94** 042318

[174] Landau D P and Binder K 2000 *A Guide to Monte Carlo Simulations in Statistical Physics* (Cambridge: Cambridge University Press)

[175] Loh E Y, Gubernatis J E, Scalettar R T, White S R, Scalapino D J and Sugar R L 1990 *Phys. Rev.* B **41** 9301–7

[176] Troyer M and Wiese U J 2005 *Phys. Rev. Lett.* **94** 170201

[177] Somma R, Nagaj D and Kieferová M 2012 *Phys. Rev. Lett.* **109** 050501

[178] Fujii K 2018 arXiv:1803.09954

[179] Seki Y and Nishimori H 2012 *Phys. Rev.* E **85** 051112

[180] Seoane B and Nishimori H 2012 *J. Phys. A: Math. Theor.* **45** 435301

[181] Seki Y and Nishimori H 2015 *J. Phys. A: Math. Theor.* **48** 335301

[182] Nishimori H and Takada K 2017 *Front. in ICT* **4** 2

[183] Jörg T, Krzakala F, Kurchan J, Maggs a C and Pujos J 2010 *Europhys. Lett.* **89** 40004

[184] Durkin G A 2018 *Phys. Rev.* A **99** 032315 (2019)

[185] Ohzeki M 2017 *Sci. Rep.* **7** 41186

[186] Hormozi L, Brown E W, Carleo G and Troyer M 2017 *Phys. Rev.* B **95** 184416

[187] Albash T 2018 *Phys. Rev.* A **99** 042334 (2019)

[188] Zurek W H and Dorner U 2008 *Phil. Trans. R. Soc.* A **366** 2953−72

[189] Dziarmaga J and Rams M M 2010 *New J. Phys.* **12** 055007

[190] Rams M M, Mohseni M and del Campo A 2016 *New J. Phys.* **18** 123034

[191] Mohseni M, Strumpfer J and Rams M M 2018 arXiv:1804.11037

[192] Kibble T W B 1976 *J. Phys. A: Math. Gen.* **9** 1387−98

[193] Zurek W H 1985 *Nature* **317** 505−8

[194] Farhi E, Goldstone J, Gosset D, Gutmann S, Meyer H B and Shor P 2011 *Quantum Information and Computation* **11** 181

[195] Dickson N G and Amin M H S 2011 *Phys. Rev. Lett.* **106** 050502

[196] Dickson N G and Amin M H 2012 *Phys. Rev.* A **85** 032303

[197] Adame J I and Mcmahon P L 2018 arXiv:1806.11091

[198] Perdomo-Ortiz A, Venegas-Andraca S E and Aspuru-Guzik A 2010 *Quant. Inf. Proc.* **10** 33−52

[199] Ohkuwa M, Nishimori H and Lidar D A 2018 *Phys. Rev.* A **98** 022314

[200] Yamashiro Y, Ohkuwa M, Nishimori H and Lidar D A 2019 arXiv:1906.10889

[201] King A D *et al* 2018 *Nature* **560** 456

[202] Demirplak M and Rice S A 2003 *J. Phys. Chem.* A **107** 9937−45

[203] Demirplak M and Rice S A 2005 *J. Phys. Chem.* B **109** 6838−44

[204] Berry M 2009 *J. Phys. A: Math. Theor.* **42** 365303

[205] Sels D and Polkovnikov A 2017 *Proc. Natl Acad. Sci.* **114** 3909

[206] Takahashi K 2013 *Phys. Rev.* E **87** 062117

[207] del Campo A 2013 *Phys. Rev. Lett.* **111** 100502

[208] Deffner S, Jarzynski C and del Campo A 2014 *Phys. Rev.* X **4** 021013

[209] Torrontegui E, Ibáñez S, Martínez-Garaot S, Modugno M, del Campo A, Guéry-Odelin D, Ruschhaupt A, Chen X and Muga J G 2013 *Shortcuts to Adiabaticity Advances in Atomic, Molecular, and Optical Physics* (Amsterdam: Elsevier) vol 62 pp 117−69

[210] Hartmann A and Lechner W 2018 *New J. Phys.* **21** 043025 (2019)

[211] Oliver W D and Welander P B 2013 *MRS Bull.* **38** 816

[212] Paik H *et al* 2011 *Phys. Rev. Lett.* **107** 240501

[213] Rigetti C *et al* 2012 *Phys. Rev.* B **86** 100506

[214] Jin X Y *et al* 2015 *Phys. Rev. Lett.* **114** 240501

[215] Yan F *et al* 2018 *Phys. Rev. Lett.* **120** 260504

[216] Orlando T, Mooij J, Tian L, van der Wal C H, Levitov L, Lloyd S and Mazo J 1999 *Phys. Rev.* B **60** 15398−413

[217] Mooij J, Orlando T, Levitov L, Tian L, van der Wal C H and Lloyd S 1999 *Science* **285** 1036−9

[218] Harris R *et al* 2007 *Phys. Rev. Lett.* **98** 177001

[219] Kerman A 2019 (in preparation)

[220] Macklin C, O'Brien K, Hover D, Schwartz M, Bolkhovsky V, Zhang X, Oliver W and Siddiqi I 2015 *Science* **350** 307

[221] Tolpygo S, Bolkhovsky V, Weir T, Johnson L, Gouker M and Oliver W 2014 *IEEE Trans. Appl. Supercond.* **25** 1101312

[222] Jurcevic P, Lanyon B P, Hauke P, Hempel C, Zoller P, Blatt R and Roos C F 2014 *Nature* **511** 202

[223] Smith J, Lee A, Richerme P, Neyenhuis B, Hess P W, Hauke P, Heyl M, Huse D and Monroe C 2016 *Nat. Phys.* **12** 907−11

[224] Maier C, Brydges T, Jurcevic P, Trautmann N, Hempel C, Lanyon B P, Hauke P, Blatt R and Roos C F 2019 *Phys. Rev. Lett.* **122** 050501

[225] Cirac J I and Zoller P 1995 *Phys. Rev. Lett.* **74** 4091

[226] Sørensen A and Mølmer K 1999 *Phys. Rev. Lett.* **83** 2274

[227] Mintert F and Wunderlich C 2001 *Phys. Rev. Lett.* **87** 257904

[228] Britton J W, Sawyer B C, Keith A C, Wang C C J, Freericks J K, Uys H, Biercuk M J and Bollinger J J 2012 *Nature* **484** 489

[229] Islam R, Senko C, Campbell W C, Korenblit S, Smith J, Lee A, Edwards E E, Wang C C J, Freericks J K and Monroe C 2013 *Science* **340** 583

[230] Richerme P, Senko C, Smith J, Lee A, Korenblit S and Monroe C 2013 *Phys. Rev.* A **88** 012334

[231] Nevado P and Porras D 2016 *Phys. Rev.* A **93** 013625

[232] Nils Trautmann P H 2018 *Phys. Rev.* A **97** 023606

[233] Friedenauer A, Schmitz H, Glueckert J T, Porras D and Schaetz T 2008 *Nat. Phys.* **4** 757

[234] Graβ T, Raventós D and Juliá-Díaz B *et al* 2016 *Nature Commun.* **7** 11524

[235] Korenblit S *et al* 2012 *New J. Phys.* **14** 095024

[236] Zhang J, Pagano G, Hess P, Kyprianidis A, Becker P, Kaplan H, Gorshkov A, Gong Z X and Monroe C 2017 *Nature* **551** 601−4

[237] Friis N *et al* 2018 *Phys. Rev.* X **8** 021012

[238] Pagano G, Hess P, Kaplan H B, Tan W L, Richerme P, Becker P, Kyprianidis A, Zhang Jand Birckelbaw E, Hernandez M Rand Wu Y and Monroe C 2018 *Quantum Science and Technology* **4** 014004

[239] Safavi-Naini A, Lewis-Swan R J, Bohnet J G, Garttner M, Gilmore K A, Jordan J E, Cohn J, Freericks J K, Rey A M and Bollinger J J 2018 *Phys. Rev. Lett.* **121** 040503

[240] Zippilli S, Johanning M, Giampaolo S M, Wunderlich C and Illuminati F 2014 *Phys. Rev.* A **89** 042308

[241] Seidelin S, Chiaverini J, Reichle R, Bollinger J J, Leibfried D, Britton J, Wesenberg J H and Blakestad R B 2006 *Phys. Rev. Lett.* **96** 253003

[242] Schmied R, Wesenberg J H and Leibfried D 2009 *Phys. Rev. Lett.* **102** 233002

[243] Frederick Hakelberg Philip Kiefer M W U W T S 2018 *Phys. Rev. Lett.* **123** 100504 (2019)

[244] Ivan A Boldin Alexander Kraft C W 2018 *Phys. Rev. Lett.* **120** 023201

[245] Soare A, Ball H, Hayes D, Zhen X, Jarratt M C, Sastrawan J, Uys H and Biercuk M J 2014 *Phys. Rev.* A **89** 042329

[246] Gorman D J, Hemmerling B, Megidish E, Moeller S A, Schindler P, Sarovar M and Haeffner H 2018 *Phys. Rev.* X **8** 011038

[247] Saffman M 2016 *J. Phys.* B **49** 202001 (2016)

[248] Jaksch D, Cirac J, Zoller P, Rolston S, Côté R and Lukin M 2000 *Phys. Rev. Lett.* **85** 2208

[249] Schauß P, Zeiher J, Fukuhara T, Hild S, Cheneau M, Macrì T, Pohl T, Bloch I and Gross C 2015 *Science* **347** 1455−8

[250] Maller K M, Lichtman M T, Xia T, Sun Y, Piotrowicz M J, Carr A W, Isenhower L and Saffman M 2015 *Phys. Rev.* A **92** 022336

[251] Jau Y Y, Hankin A M, Keating T, Deutsch I H and Biedermann G W 2016 *Nat. Phys.* **12** 71

[252] Labuhn H, Barredo D, Ravets S, de Leseleuc S, Macri T, Lahaye T and Browaeys A 2016 *Nature* **534** 667–70

[253] Pichler H, Wang S T, Zhou L, Choi S and Lukin M D 2018 arXiv:1808.10816

[254] Torggler V, Aumann P, Ritsch H and Lechner W 2018 *Quantum* **3** 149 (2019)

[255] Landig R, Hruby L, Dogra N, Landini M, Mottl R, Donner T and Esslinger T 2016 *Nature* **532** 476

[256] Kechedzhi K, Smelyanskiy V, McClean J R, Denchev V S, Mohseni M, Isakov S, Boixo S, Altshuler B and Neven H 2018 arXiv:1807.04792

[257] Jordan S P, Gosset D and Love P J 2010 *Phys. Rev.* A **81** 032331

[258] Tran T, Do M, Rieffel E, Frank J, Wang Z, OGorman B, Venturelli D and Beck J 2016 *SOCS* **16** 98–106

[259] Abbott A A, Calude C S, Dinneen M J and Hua R 2018 *International Journal of Quantum Information* **17(5)** 1950042 (2019)

[260] Mbeng G B, Fazio R and Santoro G 2019 arXiv:1906.08948 [quant-ph]

[261] Pastorello D and Blanzieri E 2019 *Quant. Inf. Proc.* **18** 303